Chemical Engineering Journal 501 (2024) 157582

Contents lists available at ScienceDirect

Chemical Engineering Journal

journal homepage: www.elsevier.com/locate/cej

Collision theory and membrane photocatalysis: Steroid hormones meet singlet oxygen in palladium-porphyrin-coated polytetrafluoroethylene membranes

Minh N. Nguyen [a], Camila S. Raota [a], Andrey Turshatov [b], Bryce S. Richards [b], Andrea I. Schäfer [a,*]

[a] Institute for Advanced Membrane Technology (IAMT), Karlsruhe Institute of Technology (KIT), Hermann-von-Helmholtz-Platz 1, Eggenstein-Leopoldshafen 76344, Germany
[b] Institute of Microstructure Technology (IMT), Karlsruhe Institute of Technology (KIT), Hermann-von-Helmholtz-Platz 1, Eggenstein-Leopoldshafen 76344, Germany

ARTICLE INFO

Keywords:
Diffusion-controlled reaction
Activation-controlled reaction
Steric factor
Rate of disappearance
Photocatalytic membrane reactor
Singlet oxygen

ABSTRACT

Photocatalytic membrane (PCM) reactors are an emerging technology for the continuous elimination of micropollutants from water. PCM material and process properties define performance limitations. A collision theory framework was established to elucidate the limiting factors of steroid hormone micropollutant photodegradation inside the pores (200 nm) of a palladium-porphyrin-coated polytetrafluoroethylene (PTFE) PCM under simulated sunlight. The collision theory can describe the degree of photodegradation of 17β-estradiol (E2). The production of singlet oxygen reactive species was limited by light intensity (up to 14 mW cm^{-2}), porphyrin loading (up to 50 μmol g^{-1}), and membrane layer thickness (46 μm, achieved *via* stacking thin membranes). Further increases in these parameters did not significantly enhance the removal of E2, because the quantity of singlet oxygen generated, and consequently the collision frequency, levelled off. Not all collisions result in photodegradation reaction. By reducing the reaction time *via* increasing the E2 molar flux, the rate of disappearance reached a threshold of 7 ± 2 nmol L^{-1} s^{-1}. This is identified as the maximum effective collision frequency, implying that 11 % of the total collisions (64 ± 5 nmol L^{-1} s^{-1}) resulted in successful reaction. The study presents a novel framework based on collision theory to predict the fundamental mechanisms of and limitations to photodegradation in porphyrin-PTFE membranes, providing unprecedented insight into the performance constraints of diverse membrane reactors for advances in materials and process engineering.

1. Introduction

Water reuse – the treatment and reclamation of wastewater for various purposes, such as irrigation, industrial processes, and even potable water production [1] – is an important strategy to achieve sustainable management of water resources and mitigation of water scarcity worldwide [2,3]. Conventional wastewater treatment plants are not designed for water reuse because they are inefficient in removing micropollutants [4,5]. Hence, these act as carriers of micropollutants into the receiving water [6]. Advanced treatment technologies are employed at the tertiary or quaternary stage to ensure that the reclaimed water meets stringent water quality standards [7]. Physical treatment technologies, such as activated carbon adsorption and membrane filtration, do not eliminate the micropollutants, but only transfer these from the water source to the activated carbon surface [8] and the concentrate stream [9], respectively. Advanced oxidation processes (AOPs), including photocatalysis, have advantages over physical treatment, such as the ability to eliminate a wide range of pollutants without the requirement of post-processing steps [10,11]. Photocatalytic processes rely on the *in situ* generation of powerful oxidising agents, such as hydroxyl radicals (•OH), superoxide anion ($•O_2^-$), and singlet oxygen ($^1O_2$), which actively attack and break the bonds within the micropollutant structures [12].

Membranes have been coupled with photocatalytic processes to degrade micropollutants in a single-pass continuous-flow configuration, in which the photocatalytic activity is maintained within short hydraulic residence times [13–15]. Inorganic photocatalysts or organic photosensitisers (PS) can be immobilised on the membrane surface and inside

* Corresponding author.
E-mail address: andrea.iris.schaefer@kit.edu (A.I. Schäfer).

https://doi.org/10.1016/j.cej.2024.157582
Received 2 August 2024; Received in revised form 10 October 2024; Accepted 9 November 2024
Available online 12 November 2024

the pore structure to avoid a photocatalyst/PS capture step [14]. Photocatalysts are substances that absorb light and participate in changing the rate of chemical transformation of the reaction partners, while PS are substances that absorb light and transfer its energy to other molecules [16]. Although PS are usually linked with medical applications, such as photodynamic therapy [17], recently, PS have been considered for the photodegradation of water-borne micropollutants [18,19].

Numerous configurations of photocatalytic membrane (PCM) reactors with immobilised photocatalysts/PS have been reported with variations in dimension, light source (light wavelength), irradiation intensity, illuminated surface area, photocatalyst/PS type, and photocatalyst/PS immobilisation on the membrane surface or within the pore structure [14,15,20]. Inside the pores of PCMs with diameters ranging from nanometres to several micrometres, the Reynolds number *Re* varies between 10^{-7} and 10^{-2}, and the flow is considered Stokes flow [21]. In this flow regime, molecules are transported radially (*i.e.* across the pore diameter) only by diffusion. The micropollutant may diffuse towards the pore walls and 'collide' (*i.e.* within a 0.3 nm proximity) with the membrane polymer (Fig. 1 A), or the surface of photocatalysts/PS immobilised on the pore surface, where reactive oxygen species (ROS) are generated (Fig. 1 B). Alternatively, the ROS can diffuse into the aqueous phase and 'collide' with micropollutants in the aqueous phase (Fig. 1 C). A collision between reactants occurs when the hydrodynamic radii of the reactants overlap each other. The probabilities of liquid-phase reactions and those at the pore depend upon how much of the reactants (both ROS and micropollutants) diffuse in the space of the pores or stay concentrated at the pore surface. The lifetime of certain ROS (such as •OH and $^1O_2$) is short and within the orders of sub-microseconds to several microseconds [22,23]. Hence, in a PCM with large (several-micrometre) pores, the ROS are more concentrated at the photocatalyst/PS surface than in the 'bulk' [24,25], resulting in poorer contact – in other words, fewer collisions – between the reactants in the aqueous phase. Under moderate confinement of 10 – 200 nm in PCMs, the observed rates of aqueous-phase reactions between small organic molecules and ROS are improved [26–28]. Further reduction of the reactor dimension to several nanometres or sub-nanometres may result in significantly enhanced reaction rates because of restricted orientations of reactant molecules and stabilisation of reactive species [29,30]. Additionally, the micropollutant and ROS instantaneously collide and interact with the reactor wall (*i.e.* photocatalyst/PS surface) [31], blurring the distinction between aqueous- and sorbed-phase reactions.

Collision theory is useful for characterising the rates of homogenous reactions [32,33] and can be applied to evaluate the performance and mechanistic limitations of PCM reactors (Fig. 1 C). The principle of collision theory is that reactants need to collide with each other to react, but only a certain number of collisions result in successful reaction. This is because the collision needs to have sufficient energy to surpass the activation energy for the reaction, *i.e.* to break the pre-existing bonds and form new bonds. Higher reactant concentrations mean more collisions within a fixed amount of time (*i.e.* a higher collision rate or collision frequency) and hence a higher reaction rate. The collision frequency is related to the reaction rate constant k (mol L^{-1} s^{-1}) *via* the Arrhenius equation [34] (see Eq. (1)).

$$k = Z\exp\left(\frac{-E_a}{R_g T}\right) \tag{1}$$

where Z (mol L^{-1} s^{-1}) is the collision frequency related to the product of the concentrations of both reactants, E_a (J mol^{-1}) is the activation energy, R_g (J K^{-1} mol^{-1}) is the ideal gas constant, and T (K) is the temperature. The term $\exp\left(\frac{-E_a}{R_g T}\right)$ denotes the fraction of collisions with sufficient energy (*i.e.* greater than E_a), which results in reaction.

In a solution mixture, each reactant molecule A is surrounded by solvent (water) molecules and travels in a 'drunken sailor' fashion (*i.e.* a Brownian motion of diffusion), as it collides with many non-reacting water molecules, continuously changing its speed and direction until it finds a reacting molecule B [35]. If the activation energy of the reaction between A and B is relatively low, the diffusion of these reactants is assumed to limit the rate of reaction (Fig. S1) [36]. Smoluchowski proposed an equation to calculate the steady-state collision frequency Z (mol L^{-1} s^{-1}) between reactants A and B in a diffusion-controlled reaction [37] (Eq. (2)).

$$Z = 4\pi(R_A + R_B)(D_A + D_B)N_{Avo}[A][B] = K_{Smol}[A][B] \tag{2}$$

where $R_A + R_B$ (m) is the radius of the collision cross-section, estimated

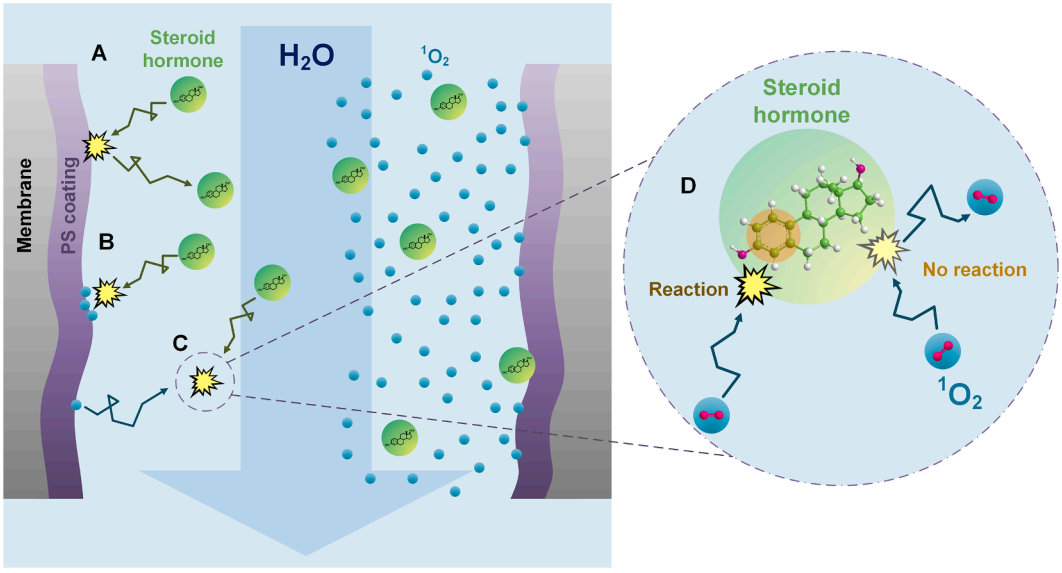

Fig. 1. Schematic of collision processes in a PCM pore with photosensitiser (PS) coating. A – Collision of a micropollutant (steroid hormone) with the pore wall (adsorption–desorption), B – Collision between a ROS (*e.g.* singlet oxygen $^1O_2$) generated on the PS surface and a micropollutant (sorbed-phase reaction), C – Collision between the ROS and micropollutant in the aqueous phase (aqueous-phase reaction), D – Magnified view of aqueous-phase collisions, highlighting the electron-rich bonds of the aromatic ring (orange circle) that is prone to reaction with $^1O_2$. (For interpretation of the references to colour in this figure legend, the reader is referred to the web version of this article.)

as the sum of the radii of reactants A and B, $N_{Avo} = 6.02 \bullet 10^{23}$ mol^{-1} is the Avogadro constant, D_A and D_B (m^2 s^{-1}) are the diffusivities of A and B, while $[A]$ and $[B]$ (mol L^{-1}) are the molar concentrations of A and B. The rate constant K_{Smol} (L mol^{-1} s^{-1}) is equal to $4\pi(R_A + R_B)(D_A + D_B)N_{Avo}$. The Smoluchowski equation was originally proposed to describe the rate of interactions between colloids in a coagulation system [37]. In that scenario, the activation energy of reaction is low as the term $\exp\left(\frac{-E_a}{R_g T}\right)$ in Eq. (1) approaches unity, and, as a result, the rate of reaction should be similar to the collision frequency ($k \approx Z$).

In real systems, the calculated collision frequency from the Smoluchowski equation is usually higher than the observed rates of reaction between molecules at varied scales (from macromolecules such as proteins [38,39] to simple organic compounds [40]). It appears that not all collisions between the reactants lead to successful reaction; for that, certain orientations of the reactant molecules relative to each other are required. In protein–protein interactions, the high specificity of the protein interaction sites [38,39] results in observed reaction rates that are several orders of magnitude lower than the collision frequency. This is attributed to a substantial 'steric factor' (between 0 and 100 %) – defined as the ratio of the experimentally determined value of the rate constant to the theoretical value predicted by the collision theory [41]. A low steric factor in protein–protein interactions corresponds to a small proportion of collisions that happen to be at the reactive sites of each reactant; as these sites occupy a small fraction of the protein sites, the probability of interaction is low [38]. In reactions between two small molecules, the steric factor may be considered as the probability of reactants to collide only at their reactive bonds [42,43]. This is illustrated in Fig. 1 D for the case of $^1O_2$ targeting the π-bonds of a steroid hormone molecule. The observed rate in such reactions can be one order of magnitude lower than the calculated collision frequency [40]. An effective collision frequency (*i.e.* the number of collisions per unit of time that leads to successful reaction) Z_{eff} (in mol L^{-1} s^{-1}) is linked with the total collision frequency Z (mol L^{-1} s^{-1}) and the steric factor β (in %) *via* Eq. (3) [43]. In a real diffusion-controlled reaction, Z_{eff} is equal to the actual rate of the reaction.

$$\beta = \frac{Z_{eff}}{Z} \tag{3}$$

To characterise the reaction kinetics in a PCM reactor *via* the collision theory, it is a prerequisite to identify and measure the concentration of the generated ROS. A collision system with only one type of ROS is easier to examine than a system in which various ROS compete for photocatalytic reaction. Common photocatalysts such as titanium dioxide (TiO_2) simultaneously generate several types of ROS (•OH, $\bullet O_2^-$, and hydrogen peroxide H_2O_2) *via* electron transfer under ultraviolet (UV) irradiation [44]. Organic PS can also participate in aerobic Type I (generation of superoxide $\bullet O_2^-$) or Type II (generation of singlet oxygen $^1O_2$) processes [45]. However, the Type I process in the case of organic PS requires the presence of an electron donor, such as amine [46], peptide [47] or iron (II) [48]. In the absence of an electron donor (as in the current investigation), only reactive $^1O_2$ is formed in a Type II process [45,49] (Fig. S2). In this case, organic PS such as porphyrins can be activated with visible light [49] as the absorption spectrum is based on the energy position of the first excited singlet state. PS efficiently undergo intersystem crossing, which facilitates energy transfer to a triplet state and subsequent energy transfer to oxygen molecules. Previous experimental investigation shows no clear evidence that ROS other than $^1O_2$ are involved in porphyrin-assisted photodegradation [50,51]. The $^1O_2$ reacts preferentially with electron-rich moieties of molecules (for example, the aromatic rings) [52,53].

With the assumption that a very small quantity of micropollutants (such as several nanograms per litre concentrations of steroid hormones) is involved in $^1O_2$ quenching, the concentration of generated ROS is determined from: i) the absorbed photon flux $\varphi_{abs,V}$; ii) the lifetime or self-decay rate of the ROS; and iii) the efficiency of photon conversion or the quantum yield Φ_Δ *via* Eq. (4) [18,54].

$$\left[{}^1O_2\right] = \frac{\varphi_{abs,V}\,\Phi_\Delta}{\left(k_\Delta + k_q[\mathrm{MP}]\right) N_{Avo}} \approx \frac{\varphi_{abs,V}\,\Phi_\Delta}{k_\Delta\, N_{Avo}} \tag{4}$$

where k_Δ (μs^{-1}) is the rate constant of $^1O_2$ decay (inverse of the $^1O_2$ lifetime), k_q (L mol^{-1} s^{-1}) is the bimolecular rate constant of $^1O_2$ quenching by micropollutant molecules, and [MP] (mol L^{-1}) is the molar concentration of micropollutants. When the micropollutant concentration [MP] is very low, $k_\Delta \gg k_q[\mathrm{MP}]$ [54]. The quantum yield Φ_Δ is defined as the ratio of the number of ROS formed to the number of photons absorbed [55]. Palladium (II)-containing porphyrins offer a high quantum yield Φ_Δ of $^1O_2$ generation [55,56] because they significantly increase spin–orbit coupling [57], which enhances intersystem crossing and makes the porphyrins more effective in generating $^1O_2$.

The incorporation of porphyrin-PS in membranes or nanofibers has been examined for the removal of dyes [58–60], steroid hormones (17β-estradiol E2, estrone E1, testosterone T, and progesterone P) [18,51,61], pharmaceuticals (parabens) [62], and pesticides (4-chlorophenol) [63]. Typically, the quantum yield Φ_Δ of porphyrins decreased when these porphyrins were incorporated in membranes, although palladium-based porphyrins were demonstrated to retain a high quantum yield Φ_Δ of 82 % [51]. With palladium porphyrin deposited in a poly(vinylidene fluoride) (PVDF) membrane support, Lyubimenko *et al.* reported high photocatalytic removal of steroid hormone micropollutants, achieving 80 – 90 % for E1 and E2 [18]. From accelerated aging tests, palladium porphyrin PCMs promise good photocatalytic function for several days to several months depending on the conditions of UV light [51,64]. However, such lifetimes are short compared to those of pristine membranes designed for pressure-driven separation, which operate for years [65].

ROS generation by immobilised porphyrins and hence the collision frequency between the ROS and micropollutants are enhanced by the light transmission capability of the membrane support. This membrane support needs to: i) absorb very little incident light itself (*i.e.* minimise parasitic optical absorption); and ii) allow significant light transmission to reach the photo-active centres deep inside the membrane [66]. Other important properties of the membrane support are high adsorption affinity for the porphyrins, and good resistance against photodegradation by UV and visible light as well as reactions with $^1O_2$ [64,67]. Symmetrical microfiltration (MF) membranes made of fluorinated polymers – such as PVDF and polytetrafluoroethylene (PTFE) – are suitable materials, as they exhibit good resistance against photodegradation [59,64,68] due to the strong C–F bonds [69], and can interact strongly with porphyrins *via* the hydrophobic effect [70].

PTFE does not absorb light in either the visible (400 – 700 nm) or UV regions (< 400 nm) [73,74]. In PTFE substrates that have pores in the micrometre range (*e.g.* standard pore sizes 1 – 20 μm and average 6 μm in Spectralon reflectance standards [77]) exhibits a > 99 % diffuse reflectance (*i.e.* incident light is almost completely scattered throughout all solid angles) [76]. Light can pass through thinner PTFE membranes with smaller pore diameters (in the nanometre range), and light transmission (in air) is influenced by morphology, such as material thickness, surface and pore roughness, pore size/porosity, and pore tortuosity [78,79]. Following pre-wetting in alcohol, PTFE thin films and membranes become partly transparent when submerged in water [71,72]. This is because PTFE thin films exhibit a low refractive index n ranging from 1.33 to 1.39 at a wavelength of 500 nm (bulk PTFE has a refractive index of 1.38) [73], which closely matches the refractive index of water [74] of 1.33. The small difference in refractive indices here ($\Delta n < 0.06$) results in better light penetration (reduced scattering), making the use of PTFE supports a better choice than PVDF (with $n \sim 1.43$ [75]).

The refractive index of porphyrin films (the literature data are available only for non-fluorinated films) is relatively high ($n = 1.5 – 3$)

[76]. This means that the loading of porphyrins (*i.e.* the molar quantity of porphyrins per unit of mass or surface area of the membrane) influences light transmission and absorption. As the thickness of the porphyrin layer – estimated to be < 20 nm depending on the loading [59] – is significantly smaller than the wavelengths of visible light, light transmission is hindered by the macroscale morphology of the supporting membrane. At higher loadings, however, scattering tends to increase due to the increased mismatch between the refractive index of water and the effective refractive index of the PTFE membrane combined with palladium porphyrin. As the concentration of porphyrin on the membrane surface further increases, concentration quenching of the porphyrin triplet state tends to occur [77], which reduces the lifetime of the triplet state and probability of $^1O_2$ photosensitisation. Additionally, porphyrin aggregation occurs. If the size of the porphyrin aggregates is larger than the diffusion length of excited electron transport, the triplet excited state is quenched before it reaches the aggregate surface and can induce $^1O_2$ generation [78]. The above phenomena can effectively decrease the $^1O_2$ concentration and, hence, collision frequency between $^1O_2$ and micropollutants. Besides, triplet–triplet annihilation phenomenon may occur and contribute to reduced excited-state lifetime and a subsequent reduction in $^1O_2$ yield [78]. However, this phenomenon will only make itself evident if the light intensity is > 10 times greater than that of terrestrial sunlight radiation [79].

The diffusion of ROS and micropollutants and subsequent collisions between these two inside the PCM pores are constrained due to the limited lifetime of the ROS and the convective transport of micropollutants in the flow. $^1O_2$ has a lifetime in water of 3.1 – 4.2 μs [54,80], which is longer than •OH lifetime at neutral pH (of around 0.2 μs [81]). As a result, $^1O_2$ exhibits a diffusion length of about 270 nm [82] (*vs.* about 70 nm for •OH). A gradient of ROS concentration with distance from the pore wall (at which the ROS are generated) can be established at steady-state conditions, under which, at any distance from the pore wall, ROS mass gain by diffusion is balanced by ROS mass loss caused by ROS self-decay plus ROS consumption by probe molecules or scavengers [26]. In a PCM with around 200 nm pore diameters, the diffusion length of $^1O_2$ (270 nm) allows this ROS to travel from the pore wall (where PS are deposited) towards the pore centre and form reaction with micropollutants in the aqueous phase. If •OH with a shorter diffusion length of 70 nm was involved, these would only concentrate at regions close to the pore walls, and reaction would not occur at the pore centre.

The flow of water through the PCM reactor determines the molar flux of the micropollutants (in mol L^{-1} s^{-1}, calculated by multiplying the water flow rate by the molar concentration of micropollutants) and hydraulic residence time (inversely proportional to the flow rate). The rate of disappearance (also in mol L^{-1} s^{-1}) is an indicator of photocatalytic degradation kinetics. It is proportional to the observed loss in micropollutant concentration and inversely proportional to the hydraulic residence time [59,83], and is assumed to be the same as the effective collision frequency Z_{eff}. A common observation with various PCM reactors is that the rate of disappearance increases with water flow rate up to a threshold, and then levels off [59,61]. This observation can be explained by the collision theory through the relationship between the molar flux of micropollutants and the maximum effective collision frequency.

In a previous extensive systematic study, the photodegradation performance in the pores was attributed to 'contact', a qualitative term that relates the hydraulic residence time in a photocatalytic membrane to the 'mixing time' (*i.e.* the average time required for micropollutants to diffuse a distance equal to half the pore diameter) [61]. While the 'contact' could explain the photodegradation performance across various pore dimensions and fluxes, it was not possible to assume the location of the reactions, or to address the limitations caused by light intensity, light penetration, photosensitiser loading, and micropollutant type. The collision theory framework applied in this work is a significant advancement in explaining all the aforementioned limiting factors, and is novel because it has not previously been applied to nanopore reactions. Specifically, the collision theory framework will be applied to elucidate how the frequency of collisions between $^1O_2$ and steroid hormone molecules, and hence steroid hormone photodegradation performance, is limited by: i) $^1O_2$ generation (with varied light intensities and porphyrin loadings); ii) optical transmission in membrane stacks (the total thickness varies from 23 to 115 μm); and iii) the molar flux of steroid hormones through the pores.

2. Materials and methods

2.1. Micropollutants and solution chemistry

Radio-labelled steroid hormones (Table S1), [6,7-^{3}H] estrone (E1) (BioTrend, Germany); [2,4,6,7-^{3}H] 17β-estradiol (E2), [1,2,6,7-^{3}H] progesterone (P), and [1,2,6,7-^{3}H] testosterone (T) (PerkinElmer, USA), were supplied as solution in ethanol. The stock solutions at a steroid hormone concentration of 10 μg L^{-1} were prepared by diluting the supplied solutions in Milli-Q water (Reference A+, Merck Millipore, USA). The feed solution containing 100 ng L^{-1} steroid hormone was prepared by diluting the stock solution in a water matrix containing background salts NaCl (10 mmol L^{-1}, prepared from analytical-grade 99.9 % (CHROMANORM) powder, VWR Prolabo, Germany) and $NaHCO_3$ (1 mmol L^{-1}, prepared from analytical-grade 99.7 % powder, Bernd Kraft, Germany); the steroid hormone concentration was made 100 ng L^{-1} by diluting the stock solution in the background electrolyte solutions. pH adjustment was performed with 1 mol L^{-1} HCl (diluted from analytical-grade HCl 37 % (ROTIPURAN), Carl Roth, Germany) and 1 mol L^{-1} NaOH (prepared from analytical-grade (EMSURE) pellets, Merck Millipore).

Some scavengers were added to the feed solution at a concentration of 10 mmol L^{-1} to determine which ROS are significant following a previously published procedure [84]. Briefly, isopropanol (IPA, > 99.8 %, HPLC grade, VWR, Germany), p-benzoquinone (p-BQ, > 98 %, Thermo Scientific Chemicals, Germany), furfuryl alcohol (FFA, 98 %, Thermo Scientific Chemicals) and sodium oxalate (SO, 99 %, Thermo Scientific Chemicals) are scavengers for •OH, $•O^{2-}$, $^1O_2$ and photo-induced electron holes (h^+), respectively. The concentration of scavenger of 10 mmol L^{-1} is much higher than that of steroid hormone (0.37 nmol L^{-1}), and this scavenger should dominate completely in interaction with the reactive species.

2.2. Porphyrin incorporation in PTFE membranes and porphyrin loading determination

The pristine PTFE membranes, commonly used as filters in organic solution and gas purification, were supplied by Merck Millipore, USA (batch 21012441–0101). It is noted that the methods and fundamentals investigated are not limited to PTFE and PVDF, given that concerns have emerged over the production of harmful poly- and perfluoroalkyl substance (PFAS) by-products from PTFE/PVDF [85], which will lead to a phasing out of such membranes. Findings in this work are potentially transferrable to other types of support materials as long as these interact with porphyrins. The PTFE membranes have a nominal pore diameter of 0.2 μm and thickness of 23 μm.

The porphyrin incorporated into the PTFE membranes is (5,10,15,20-tetrakis(pentafluorophenyl)-21H,23H-porphine palladium (II) (PdTFPP, > 94 %, Frontier Specialty Chemicals, USA). The photocatalytic PdTFPP-PTFE membranes were produced following the protocol described by Lyubimenko *et al.* for PdTFPP-PVDF membranes [59,61]. The PTFE membrane coupons with 25 mm diameter were submerged and sonicated in acetone (99 %, Merck Millipore) for 8 min in a beaker placed in an ultrasonic bath (Model USC 300 T, VWR, Germany). Subsequently, the coupons were removed, rinsed with methanol (>99 %, Merck Millipore), dried for 10 min in air at room temperature, and then placed in a custom-built six-well stainless-steel plate. In a glass beaker, PdTFPP was dissolved in tetrahydrofuran (THF, 99.9 %, Merck

Millipore) to form a PdTFPP solution of concentration between 1 and 30 mmol L^{-1}. An aliquot of 1.5 mL of this solution was added to each well of the stainless-steel plate containing the PTFE membrane coupon. The wells were then capped to avoid solvent evaporation, and the stainless-steel plate was shaken for 4 h on a bench-top shaker (Shaker KM-2, Edmund Büchler, Germany). The PdTFPP-coated coupons were then washed with Milli-Q water (Reference A+, Merck Millipore, with resistivity > 18.2 MΩ cm^{-1}) to remove free (*i.e.* un-adsorbed) porphyrins, and sonicated in Milli-Q water for 8 min so that the solvent in the membrane pores is displaced by water. The porphyrin membranes were then stored in Milli-Q water until the experiment. In a thin membrane (< 30 μm in thickness), it is expected that the distribution of PdTFPP along the membrane thickness is roughly uniform [61]. This is not the case for thicker membranes (*e.g.* PVDF membrane with 110 μm thickness), as the PdTFPP concentrations near the top and bottom surfaces of the membrane are two to five times higher than in the bulk of the membrane [59].

Porphyrin loading determination was performed *via* three methods: 1) mass balance; 2) determination from the washing solution; and 3) weight gain. The mass balance method (method 1) did not yield significant loading results due to the negligible difference in porphyrin solution absorbance before and after the loading (Figs. S3 and S4). Hence, methods 2 and 3 were considered as alternatives. A description of the three methods is given in Supplementary Section 3. Method 2 relies on the condition that PdTFPP was fully washed off the membrane by THF solvent. Method 3, on the other hand, requires careful operation and high sensitivity of the analytical balance. Method 2 (washing) and method 3 (weight gain) yield significant and comparable loading results (Fig. S5), thus both can be used for loading determination. For method 2, the absorptance spectrum indicates insignificant presence of PdTFPP remaining in the membrane after washing (see Fig. S6), hence this method is valid for the thin PTFE membranes. At a porphyrin concentration in the well of 13.9 ± 0.5 mmol L^{-1}, the corresponding loading in the PTFE membrane (around 10 mg in mass) is 50 ± 10 μmol g^{-1}. The adsorbed porphyrin accounts for 2.4 – 2.9 % of the total mass in the well. The loading values reported in this paper were determined with method 2.

2.3. Photocatalytic experiment procedure

Steroid hormone photodegradation experiments were performed in a PCM reactor system with an active filtration area of 2.0 cm^2 and a quartz window (2 cm in thickness and 1.7 cm^2 in area) as illustrated in Fig. S7 and described in a previous study [18].

Light from a solar simulator (SolSim SINUS-70, WaveLabs, Germany) was calibrated using a reference to the air mass 1.5 global spectrum (AM1.5G, 350 – 1150 nm) [86] using the auto-calibration tool from the WaveLabs software (Fig. S8). The output spectrum (350 – 1150 nm) has a maximum intensity of 81.5 mW cm^{-2}, as this corresponds to the 350 – 1150 nm fraction of the entire AM1.5G solar spectrum (280 – 4000 nm) [51], which has an intensity of 100 mW cm^{-2}. The filtration protocol is the same as described by Lyubimenko *et al.* [18] and summarised in Table S2. Unless indicated otherwise, the experiments were performed at a light irradiation intensity of 14 mW cm^{-2} (14 % of terrestrial sunlight), a water flux of 600 L m^{-2} h^{-1} (corresponding feed flow rate of 2 mL min^{-1}), 100 ng L^{-1} steroid hormone (E2) concentration, a solution pH of 8.2 ± 0.1, and a temperature of 24.0 ± 0.2 °C. The room temperature (controlled with air conditioning) and humidity were monitored as shown in Fig. S9.

2.4. Characterisation of membrane surface and optical properties

The contact angle of the PTFE membrane support was indicated with both the sessile drop and captive bubble method (Drop Shape Analyser DSA25, Krüss) to characterise the surface properties of the PTFE membranes. The sessile-drop method is more suitable for characterising hydrophobic surfaces, while the captive-bubble method is more suitable for hydrophilic or aerophobic surfaces. The hydrophobicity and aerophobicity of PTFE surfaces depend on the wetting [87,88].

In the sessile drop method, a pure water drop of 5 μL was released from a 21G needle with an inner diameter of 0.514 mm onto a dry membrane piece. In the captive bubble method, the membrane piece was submerged in a) Milli-Q water and b) methanol (and then thoroughly rinsed with Milli-Q water) for 24 h before characterisation. An air bubble (8 μL) was released from a J-shaped needle (diameter 0.493 mm) onto the wetted surface. The equipment software (ADVANCE, Krüss) calculated the contact angles in both cases. Results are shown in Figs. S10 and S11. Captive bubble results depend on whether the surface of the PTFE membrane is properly wetted. If the surface is not wetted (*i.e.* air is trapped in the pores) the air bubble may dissipate on the surface; if the surface is properly wetted, the air bubble would stay on the surface (see Fig. S12) [88].

The porosity of PTFE was determined *via* helium pycnometry (Pycnomatic ATC, Porotec, Germany). Pycnometry detects all void volumes that helium atoms can penetrate, gives precise and reproducible results, and does not distort membranes due to high pressures (compared to mercury intrusion, for instance) [89]. A PTFE membrane sample with a mass of 343 mg (measured on an analytical balance) was characterised with multiple (27) cycles/repeats to determine the porosity and variation in porosity. An average porosity of (57 ± 1) % was indicated (Fig. S13).

The absorbance spectra of pristine and coated membranes were obtained in a spectrophotometer with an integrating sphere (Cary 7000, Agilent, USA). Membranes were placed inside a quartz cuvette (40 mm • 40 mm and light path 10 mm, Starna Scientific, Germany) containing water. The wavelength range was set at 300 – 1200 nm. The scan rate was 600 nm min^{-1} in UV–Vis and 300 nm min^{-1} in near infra-red (NIR) regions. The signal averaging time was selected at 0.1 s in UV–Vis and 0.2 s in NIR, and the switch between UV–Vis and NIR detectors occurred at the 860 nm wavelength. The spectral bandwidth was independently fixed at 4 nm in both UV–Vis and NIR to avoid both excessive noise and a step in the data in the detector changeover region. The latter occurs when the spectral bandwidth is allowed to vary, which in turn results in a smaller or larger area of the sample being illuminated. This behaviour results in a different spectrophotometric value being measured for non-uniform samples. The baseline calibration was performed with 0 % and 100 % transmittance. Transmittance and absorptance with a water-filled cuvette (no membrane) were measured on each day of analysis. For the absorptance (***A***%) measurement, the cuvette was mounted in the centre of the integrating sphere. The Cary WinUV software (Agilent) calculated ***A***% by subtracting the transmitted and reflected light. For transmittance (***T***%) measurement, the cuvette was placed just outside of the integrating sphere. The Cary WinUV software determined ***T***% from the light that entered the integrating sphere.

If the membrane was not properly wetted (*e.g.* without filling the hydrophobic pores with water), the light transmittance would decrease (Fig. S19) due to the mismatch between the refractive indices of air and PTFE. Air had to be removed with the use of solvents to ensure reproducible light transmittance results. The uncoated PTFE membrane was pre-wetted in methanol for 15 min prior to the optical measurement. During the preparation of PCMs, the PTFE membranes were conditioned in THF and methanol. The resulting PdTFPP-PTFE membranes were kept submerged in water at all the time.

2.5. Analytical methods

Radio-labelled hormones in feed and permeate samples are quantified with ultra-high performance liquid chromatography coupled with flow scintillation (UHPLC-FSA, Perkin Elmer, USA) according to the methodology adapted from Lyubimenko *et al.* [18]. A change from the published method is that the UHPLC flow rate was set at 0.2 mL min^{-1} instead of 0.25 mL min^{-1}, and injection volume was increased from 100

to 200 μL (with a larger injection loop volume of 200 μL) to increase the peak area in chromatograms. Additionally, the composition of methanol/water in the gradient from 40/60 to 80/20 is increased within a shorter time (at 15 min) for E1 and E2 but maintained at 25 min for T and P. This change allows speeding up the analytical time for E1/E2 compared with Lyubimenko *et al.* [18], as these analytes elute faster without compromising peak area [90]. The detection limit is < 5 ng L^{-1} for all steroid hormones, similar to the value reported by Lyubimenko *et al.* (3.4 ng L^{-1}) [18]. In the FSA, the eluent was mixed with scintillant (Ultima-Flo M, Perkin Elmer) at a scintillant flow rate of 4 mL min^{-1} for steroid hormone counting. The steroid hormones were eluted at 17.1, 17.3, 18.4, and 23.6 min for E1, E2, T, and P, respectively, and separated from breakdown products in a C18 column (Kinetex, 150 mm length & 2.1 mm diameter, silica particle diameter 1.7 μm, Phenomenex, USA, kept at a fixed temperature of 50 °C). The breakdown products were not identified but eluted earlier than the steroid hormones.

Liquid scintillation counting (LSC, 2550 TR/AB, PerkinElmer) was used to determine the total activity of tritium in a mixture of radiolabelled steroid hormones and degradation products. As HPLC-FSA allows the quantification of undegraded steroid hormones, a combination of LSC and HPLC-FSA can be used to distinguish adsorption and photodegradation [91]. For LSC, a sample volume of 1 mL was mixed with 1 mL of scintillation cocktail (Optiscint LLT, PerkinElmer). The activity measurement was performed in triplicate, each with a counting time of 10 min [92]. Instrument calibration with tritium-labelled E2 standard shows a linear relationship between activity and E2 concentration between 0.1 and 100 ng L^{-1}. The limit of detection is 0.1 ng L^{-1} of E2, corresponding to around $1 \cdot 10^{-3}$ nmol L^{-1} of tritium.

pH was determined with a SenTix 81 electrode (WTW, Germany) connected to a pH/conductivity meter (pH/cond 3320, WTW). Dissolved oxygen (DO) content was determined with an FDO-925 electrode (WTW) connected to a Multi 3620 IDS device (WTW). Before each DO measurement, the electrode was inserted in an air-saturated vessel (FDO Check, WTW) to check the DO at 100 % saturation. This DO content should vary between 8.3 mg L^{-1} (at 25 °C) and 9.0 mg L^{-1} (at 20 °C) to indicate that the electrode was functional. The feed pH and DO concentrations measured before each experiment are reported in Fig. S9.

To determine the concentration of $^1O_2$, firstly the absorbed photon flux per membrane area, $\varphi_{abs,A}$, was estimated from the absorptance of light at all wavelengths in the range of 350 – 800 nm according to Eq. (5) assuming that the amount of PdTFPP and DO were not limiting factors.

$$\varphi_{abs,A} = \int_{\lambda=350\ \mathrm{nm}}^{800\ \mathrm{nm}} \varphi_{inc,\lambda}\ \alpha_\lambda\ d\lambda \tag{5}$$

where $\varphi_{inc,\lambda}$ (photons m^{-2} s^{-1} nm^{-1}) is the incident photon flux, as reported in a previous publication [18], and α_λ (between 0 and 100 %) is the absorptance of light at each wavelength λ. The absorbed photon flux per reactor volume $\varphi_{abs,V}$ (photons L^{-1} s^{-1}) was related to $\varphi_{abs,A}$ *via* Eq. (6).

$$\varphi_{abs,V} = \frac{\varphi_{abs,A}\ A_m}{V_m} = \frac{\varphi_{abs,A}}{h} \tag{6}$$

where A_m (m^2) is the effective membrane area for filtration, and V_m (L) is the dimensional volume of the membrane and is equal to A_m multiplied by membrane thickness h (m). The molar concentration [$^1O_2$] (mol L^{-1}) was determined from Eq. (4) [18,54], under the assumptions that: i) all PS molecules in the thin layer (23 μm) membrane could generate $^1O_2$ with constant quantum yield; and ii) the lifetime of $^1O_2$ inside the membrane was similar to that in the bulk water. The $^1O_2$ quantum yield of incorporated PdTFPP Φ_Δ is equal to 82 % (value is for PdTFPP on PVDF, and it is assumed that the value for PdTFPP on PTFE is similar) [59], and the self-decay rate constant k_Δ is equal to 0.33 μs^{-1} (inverse of the average $^1O_2$ lifetime).

For establishing the collision theory, [$^1O_2$] was assumed to not vary with distance from the pore wall. This assumption is plausible because in the absence of any significant scavengers and at steady state, [$^1O_2$] at the pore centre (100 nm from the wall) was slightly lower (18 %) than [$^1O_2$] at the pore wall, where $^1O_2$ was generated (see Fig. S14).

Additionally, by pre-saturating the membranes with steroid hormones in the dark phase, the steroid hormone concentration was assumed to be largely uniform in the radial direction (see Fig. S15), while the low adsorption affinity allowed membrane saturation to be reached quickly (Fig. S16), within 100 mL of filtration in the dark phase for E2. Based on tritium analysis, the adsorption of both steroid hormones (E2) plus degradation products was found to reach saturation relatively quickly within 600 mL of filtration in the light phase (see Fig. S17). Hence, a uniform distribution of steroid hormones in the radial direction was also assumed in the light phase.

2.6. Calculations and error analysis

The equations used in calculations are as shown in Table S3. Error analysis is described in Tables S4 and S5. The main contributor to feed hormone concentration error comes from the analysis (10 % uncertainty), and the main factors contributing to permeate hormone concentration error are analysis (10 – 35 % uncertainty; higher uncertainty was attained at lower concentrations), membrane coupon variation (around 10 % variation in permeability) and variations in flux, pressure, and temperature (7 – 10 % in combination). The error in $^1O_2$ concentration is assumed to be 10 % based on the variation in porphyrin loading.

3. Results and Discussions

This paper seeks to elucidate the limiting factors behind the collision frequency between $^1O_2$ and steroid hormone molecules – hence the steroid hormone removal. First, the limitations of light intensity and PdTFPP loading were examined for the removal of E2. Next, the total membrane thickness (*i.e.* the number of membranes in a stack between 1 and 5) was varied to inspect how the membrane optical properties influenced E2 removal. Subsequently, the limitation of water flux (and steroid hormone molar flux) was evaluated to determine an effective collision frequency threshold Z_{eff}, and the percentage of collisions that led to E2 elimination reaction (*i.e.* the steric factor). Finally, from photocatalytic experiments with varied steroid hormone types (E1, E2, T and P), the selectivity towards micropollutants with an aromatic ring was examined *via* the effective collision frequency.

3.1. Collision frequency limited by the incident light intensity

Because the amount of $^1O_2$ generated is determined by the number of absorbed photons, the light intensity was varied to determine the threshold of light intensity, and hence the incident photon flux, above which photon absorption no longer limited E2 photodegradation. An examination of reactive species types was done *via* the introduction of scavengers; results are shown in Fig. S18 indicating that $^1O_2$ was the only significant reactive species in the system (the experimental parameters of this experiment are shown in Fig. S23). The relative steroid hormone concentration, presented as permeate concentration c_p divided by feed concentration c_f, was plotted against the permeate volume V_p in Fig. 2 A. Steroid hormone removal R and apparent rate of disappearance $\bar{r}$ *vs.* light intensity at the same flux (600 L m^{-2} h^{-1}) and loading (50 ± 10 μmol g^{-1}) are shown in Fig. 2 B. The experimental parameters are shown in Fig. S24.

From Fig. 2 A, E2 adsorption saturation (where $c_p/c_f \sim 1$) was reached in the dark phase (100 mL), and the steady-state concentration of E2 (c_p/c_f = constant) was reached within 600 mL of the light phase in all experiments. Without irradiation (*i.e.* the light intensity was 0 mW cm^{-2}), E2 removal was not observed as the permeate concentration was

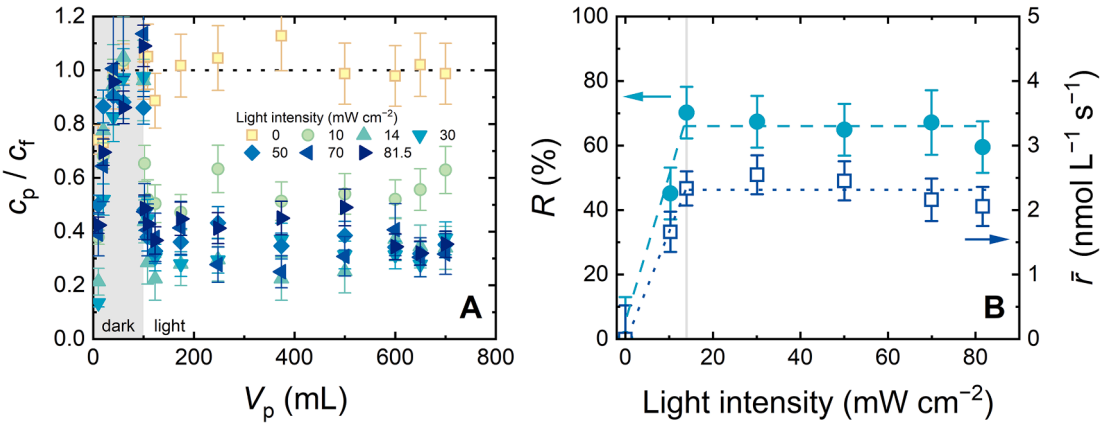

Fig. 2. c_p/c_f as a function of V_p (A); R and $\bar{r}$ as functions of light intensity (B). PdTFPP loading 50 ± 10 μmol g^{-1}, flux 600 L m^{-2} h^{-1}, 100 ± 10 ng L^{-1} E2, 10 mmol L^{-1} NaCl, 1 mmol L^{-1} $NaHCO_3$, 8.5 ± 0.3 mg L^{-1} dissolved oxygen, pH 8.2 ± 0.1.

equal to the feed concentration, resulting in $c_p/c_f = 1$. The relative concentration c_p/c_f decreased to around 0.6 at an increased light intensity of 10 mW cm^{-2}. As the light intensity further increased from 14 to 81.5 mW cm^{-2}, c_p/c_f only varied slightly, between 0.3 and 0.4. Fig. 2 B shows an initial increase in E2 removal at steady state, from 0 to 70 %, with the light intensity increasing from 0 to 14 mW cm^{-2}. The corresponding rate of disappearance increased from 0 to 2.4 nmol L^{-1} s^{-1}. This means, when more photons were absorbed, a higher quantity of $^1O_2$ was produced, which led to more collisions between E2 and $^1O_2$ and hence higher E2 removal. However, when the light intensity increases from 14 to 81.5 mW cm^{-2} (the latter value is the light intensity of terrestrial sunlight), E2 removal and rate of disappearance did not vary significantly, meaning that the light intensity was no longer a limiting factor. The flattening of the photodegradation curve above a certain light intensity is similar to the observations for PdTFPP-PVDF membranes in previous experimental work [18,59], and could be attributed to either the limited amount of DO or the limited number of photocatalytic centres (PdTFPP) [59]. The amount of DO (which is present in the solution at a concentration of 8 – 9 mg L^{-1} (equivalent to a molar concentration of 0.25 – 0.28 mmol L^{-1}), see Fig. S9) is not likely to limit the amount of $^1O_2$ produced (which is calculated with Eq. (4) to be in the order of 17 nmol L^{-1} at a light intensity of 14 mW cm^{-2}). Therefore, it is hypothesised that the quantity of photocatalytic centres (*i.e.* the PdTFPP) limited the generation of $^1O_2$. The similar behaviour (flattening of the degradation curve) has often been observed for catalytic reactions in membrane reactors [93,94], and has been similarly attributed to the limited number of photocatalytic centres available on the surface.

When the incident photon flux was a limiting factor, with increasing light intensity from 0 to 14 mW cm^{-2}, the collision frequency that is correlated with the incident photon flux increased from 0 to 64 nmol L^{-1} s^{-1} (Eq. (2)). To ensure good steroid hormone removal while preventing wasting photon energy, in the experiments with other varied parameters, the light intensity will be fixed at 14 mW cm^{-2}. In the next step, the PdTFPP loading will be varied between 3 and 105 μmol g^{-1} to examine whether PdTFPP loading limited $^1O_2$ generation and the frequency of collisions between $^1O_2$ and E2.

3.2. Collision frequency limited by the porphyrin loading

If light intensity is no longer a limiting factor (at 14 mW cm^{-2}) and $^1O_2$ generation is limited by the quantity of PdTFPP, the quantity of photons absorbed by PdTFPP will increase with increasing PdTFPP loading. To examine how photodegradation performance was influenced by PdTFPP loading, E2 removal and apparent rate of disappearance *vs.* light intensity at varied PdTFPP loadings and the same flux (600 L m^{-2} h^{-1}) are shown in Fig. 3. The experimental parameters are shown in Fig. S25.

From Fig. 3 A, E2 adsorption saturation was reached in the dark phase, and steady-state concentration of E2 was reached within 600 mL of the light phase in all experiments. As seen in Fig. 3 B, with an increase in the PdTFPP loading from 0 to 50 μmol g^{-1}, E2 removal increased from 3 to 70 %, and the rate of disappearance from 0.83 to 2.4 nmol L^{-1} s^{-1}. With a further rise in PdTFPP loading from 50 to 88 μmol g^{-1}, E2 removal and rate of disappearance reached a plateau at around 70 % and 2.4 nmol L^{-1} s^{-1}, respectively. The above observations may suggest $^1O_2$

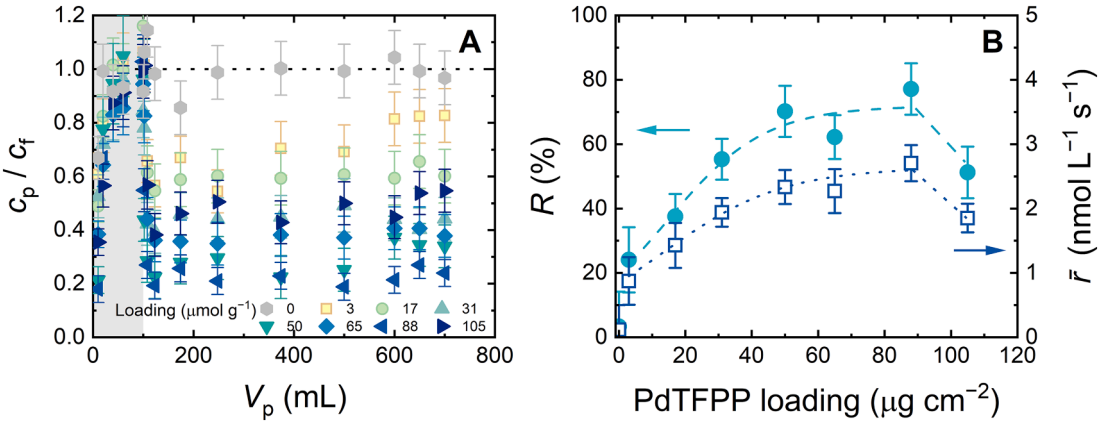

Fig. 3. c_p/c_f as a function of V_p (A); R and $\bar{r}$ as functions of PdTFPP loading (B). Light intensity 14 mW cm^{-2}, flux 600 L m^{-2} h^{-1}, 100 ± 10 ng L^{-1} E2, 10 mmol L^{-1} NaCl, 1 mmol L^{-1} $NaHCO_3$, 8.5 ± 0.3 mg L^{-1} dissolved oxygen, pH 8.2 ± 0.1.

generation and the collision frequency were limited by PdTFPP loading in the lower range of loadings (0 – 50 μmol g^{-1}), and was no longer in the loading range of 50 – 88 μmol g^{-1}. It is further noted that at a very high PdTFPP loading of 105 μmol g^{-1}, the E2 removal and rate of disappearance reduced to 51 % and 1.9 nmol L^{-1} s^{-1}, respectively. This lower photodegradation performance can be explained by i) concentration quenching of the PdTFPP triplet state [77] (hence reduced $^1O_2$ sensitisation), and ii) porphyrin aggregates in which triplet states formed in the bulk of the aggregates are quenched before reaching the surface of the aggregate for $^1O_2$ generation [78].

To explain the trend in E2 removal with PdTFPP loading *via* the collision theory, light absorptance and transmittance of the PdTFPP-PTFE PCMs with varied PdTFPP loadings are reported in Fig. 4 A, and the absorptance was used to calculate the molar concentration of $^1O_2$ and collision frequency (reported in Fig. 4 B). The absorptance and transmittance of a pristine membrane without any PdTFPP are shown in Fig. S19. It is noted that light absorption of the pristine membrane in the range of 350 – 1150 nm was minimal; and the remaining absorption was probably parasitic absorption; as a result, the quantity of $^1O_2$ generated was insignificant (~ 0 nmol L^{-1}).

From Fig. 4 A, it can be seen that the absorption maxima of the PdTFPP-PTFE PCMs at 518 and 550 nm peaks reached around 91 – 92 % at a loading of 31 μmol g^{-1}, after which only a minor increase was observed (to 95 %) with increasing loading from 31 to 105 μmol g^{-1}. From Fig. 4 B, transmittance at wavelengths 600 – 900 nm and 450 – 480 nm decreased by increasing PdTFPP loading from 3 to 105 μmol g^{-1}. The transmittance at two of the absorption peaks of PdTFPP (518 and 550 nm) decreased to a minimal value of 3 % with an increasing loading from 3 to 50 μmol g^{-1}, and remained at < 5 % with a further increase in loading from 50 to 105 μmol g^{-1}. Because the refractive index of PdTFPP ($n = 1.5 – 3$ [76]) is higher than that of PTFE ($n \sim 1.38$ for bulk material [73]) and water ($n = 1.33$ [74]), the effective refractive index of PdTFPP combined with PTFE may increase with PdTFPP quantity and intensify the mismatch in refractive index between water and the PdTFPP-PTFE surface. This may explain the decline in light transmittance with increasing PdTFPP loading. The optical characterisation results correspond with visual inspection of the membranes. At loadings of 31 – 105 μmol g^{-1}, the membrane colour was the same, and it was impossible to distinguish the membranes (Fig. S20).

From Fig. 4 C, the steady-state molar concentration of $^1O_2$ generated increased from 5.6 to 18 nmol L^{-1} with increasing loading from 3 to 31 μmol g^{-1}, but from 31 to 105 μmol g^{-1}, only a relatively small increase in $^1O_2$ molar concentration was observed (from 18 to 22 nmol L^{-1}). This slight increase is because the absorptance at some wavelength ranges (such as the one between 440 and 490 nm) other than the absorption peaks of PdTFPP increased with loading, and hence the absorbed photon flux (calculated *via* Eq. (6)) also increased. As a result, more $^1O_2$ was generated. The same trend was observed for the collision frequency (Fig. 4 D), which appeared to reach a maximum at around 85 nmol L^{-1} s^{-1} at high loadings (65 – 105 μmol g^{-1}). It is implied that the number of photocatalytic centres above 31 – 50 μmol g^{-1} loadings minimally affected the frequency of collisions between $^1O_2$ and E2.

3.3. Variation of collision frequency with light penetration in membrane

By stacking PCMs at the same loading (50 ± 10 μmol g^{-1}), the number of photocatalytic centres is increased; however, light transmission through the next membrane in the stack is decreased due to light absorption by PdTFPP and light scattering. As a result, the quantity of $^1O_2$ generated would reduce in this membrane layer. The changes in relative concentration with permeate volume and E2 removal evaluated with varying PCM stack thicknesses are shown in Fig. 5. The experimental parameters are shown in Fig. S26.

From Fig. 5 A, with all the membrane stacks, the saturation of E2 adsorption was reached within the dark phase, and a steady state concentration was reached within 600 mL in the light phase. As observed in Fig. 5 B, E2 removal did not vary significantly with the number of PCMs in the stack (between 70 % and 85 %, with an error bar of around 8 %),

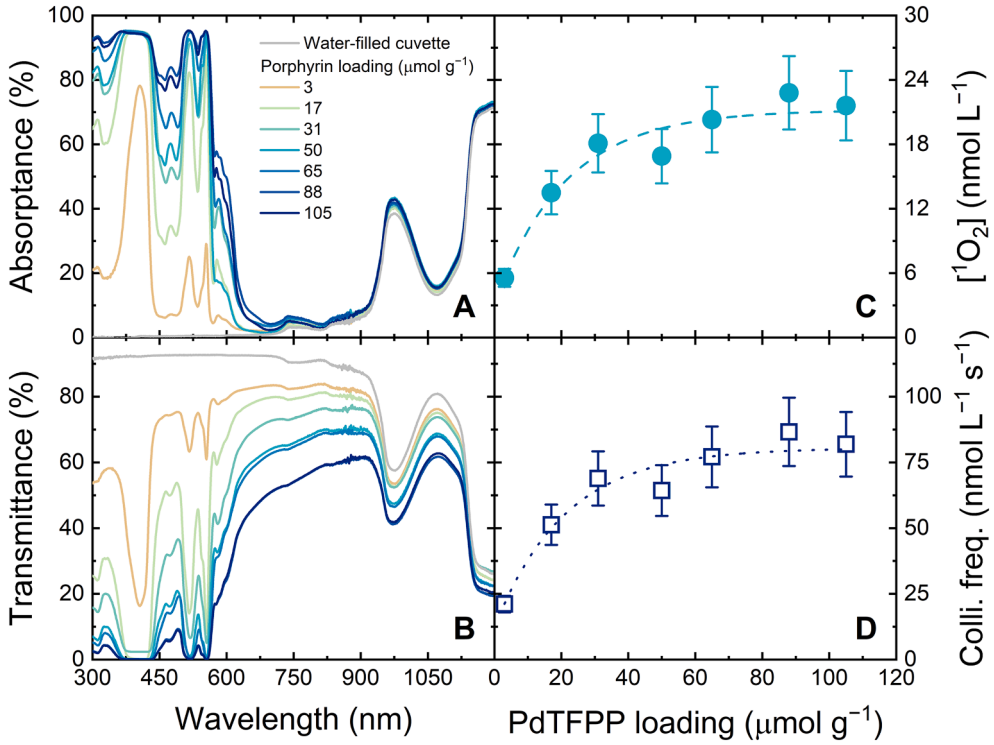

Fig. 4. Absorptance (A) and transmittance (B) *vs*. wavelength at varied porphyrin loadings. Molar concentration of singlet oxygen generated [$^1O_2$] (C) and frequency of collisions between $^1O_2$ and E2 (D). Conditions for C & D: light intensity 14 mW cm^{-2}, flux 600 L m^{-2} h^{-1}, 100 ± 10 ng L^{-1} E2, 10 mmol L^{-1} NaCl, 1 mmol L^{-1} $NaHCO_3$, 8.5 ± 0.3 mg L^{-1} dissolved oxygen, pH 8.2 ± 0.1.

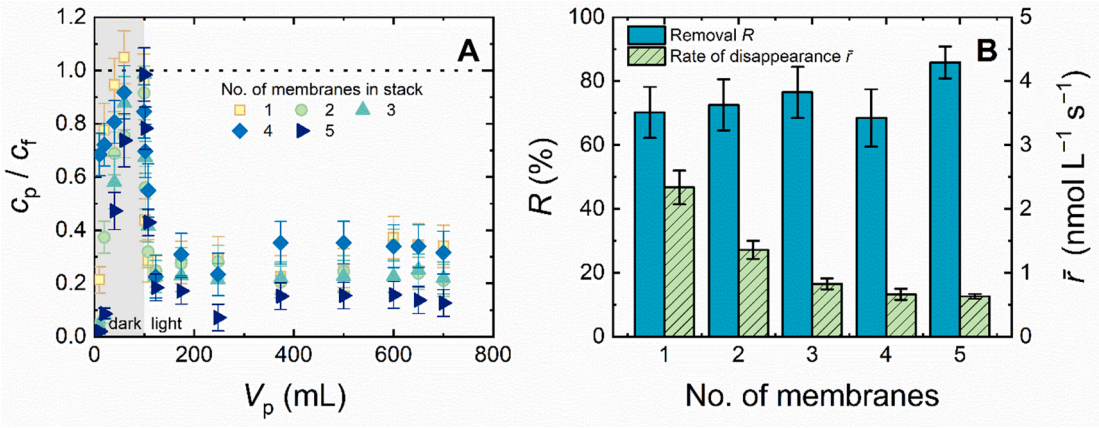

Fig. 5. c_p/c_f as a function of V_p (A); R and $\bar{r}$ as functions of the number of membranes in the stack (B). PdTFPP loading 50 ± 10 μmol g^{-1}, light intensity 14 mW cm^{-2}, flux 600 L m^{-2} h^{-1}, 100 ± 10 ng L^{-1} E2, 10 mmol L^{-1} NaCl, 1mmol L^{-1} $NaHCO_3$, 8.5 ± 0.3 mg L^{-1} dissolved oxygen, pH 8.2 ± 0.1.

which means that the PCM thickness did not limit the photocatalytic degradation of E2. On the other hand, the rate of disappearance decreased with increasing PCM thickness as a result of increasing hydraulic residence time.

The removal results with varied PCM thickness imply that the increased quantity of photocatalytic centres (number of PdTFPP molecules) would not correspond to some improvement in the photocatalytic performance when light did not effectively reach the PdTFPP in the subsequent layers. It is hypothesised that light absorption in the first membrane layer was effective, and a much smaller fraction of photons could reach the second layer, and so on. To examine this hypothesis, the absorptance and transmittance of PCM stacks, and the molar concentration of $^1O_2$ and collision frequency in each layer are shown in Fig. 6. The optical properties of the corresponding blank membrane stacks are shown in Fig. S21, highlighting a decrease in transmittance in subsequent membrane layers due to light scattering.

From Fig. 6 A, adding a second PCM did not impact the absorptance at the absorption peaks of PdTFPP (518 and 550 nm), but the absorptance was significantly higher in other wavelength ranges (440 – 490 nm and 570 – 600 nm) compared with that of a single PCM. However, adding further membrane layers in the stack did not result in a significant increase in absorptance at the 440 – 490 nm region. Fig. 6 B shows that transmittance decreased with increasing PCM layer thickness as a result of increased light scattering.

The analysis of $^1O_2$ molar concentration was done for each individual layer, by finding the total $^1O_2$ concentration generated for the cumulative thickness, and subtracting this value by the total $^1O_2$ concentration with one fewer PCM layer. The molar concentration of E2 in the subsequent layer was also calculated for each individual layer in the same manner. Fig. 6 C shows that while 17 nmol L^{-1} of $^1O_2$ was generated in

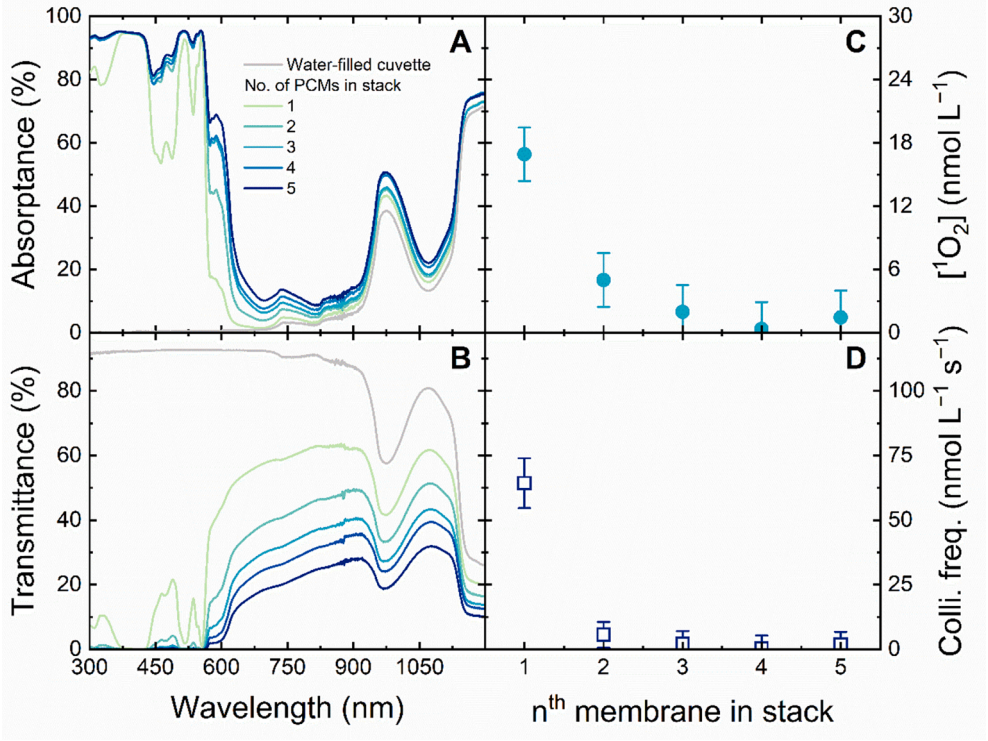

Fig. 6. Absorptance (A) and transmittance (B) *vs.* wavelength at varied numbers of membranes in the stack. Molar concentration of singlet oxygen [$^1O_2$] (C) and frequency of collisions (D) in each layer of the stack. Conditions for C & D: PdTFPP loading 50 ± 10 μmol g^{-1}, light intensity 14 mW cm^{-2}, flux 600 L m^{-2} h^{-1}, 100 ± 10 ng L^{-1} E2, 10 mmol L^{-1} NaCl, 1 mmol L^{-1} $NaHCO_3$, 8.5 ± 0.3 mg L^{-1} dissolved oxygen, pH 8.2 ± 0.1.

the first layer, only around 5 nmol L^{-1} was generated in the second layer, and insignificant amounts in the third, fourth, and fifth layers (insignificance is indicated when the error is larger than the value). In Fig. 6 D, the collision frequency was only significant in the first layer, because of the depletion of both E2 and $^1O_2$ molecules (the latter is due to insufficient light reaching the below layers). These results show that adding PCM and hence increasing the layer thickness up to 115 μm did not enhance the photocatalytic performance significantly, because effective light absorption was already achieved within the top-most PCM layer (23 μm in thickness).

3.4. Determination of an effective collision frequency threshold

In the previous experiments, the water flux was fixed at 600 L m^{-2} h^{-1} corresponding to a uniform E2 molar flux of 4.7 nmol L^{-1} s^{-1}. This molar flux is much lower than the collision frequency in the order of 65 – 90 nmol L^{-1} s^{-1}, hence the reaction time in the PCM might not limit the chance of collisions. By increasing the water flux and hence the molar flux of E2, the rate of photocatalytic reaction may be limited by the faster E2 replenishment. The limitation threshold is a value in E2 molar flux that is roughly equal to the frequency of successful collisions Z_{eff} as well as the threshold for the rate of disappearance. To determine Z_{eff}, the water flux was varied between 60 and 3000 L m^{-2} h^{-1} by adjusting the flow rate with the HPLC pump between 0.2 and 10 mL min^{-1}. The corresponding E2 molar flux (assuming that the molar flux of E2 did not account for the mass loss caused by adsorption and degradation) varied between 0.47 and 23 nmol L^{-1} s^{-1}. E2 removal and rate of disappearance *vs.* E2 molar flux are shown in Fig. 7. The dependence of hydraulic residence time on the water flux and E2 molar flux is shown in Fig. S22. The experimental parameters are shown in Fig. S27.

From Fig. 7 A, E2 adsorption saturation was reached within the dark phase, and a steady state concentration was reached within 600 mL in the light phase. Fig. 7 B shows that similar E2 removal results were achieved within an E2 molar flux range between 0.47 and 9.3 nmol L^{-1} s^{-1} (corresponding to a water flux range between 60 and 1200 L m^{-2} h^{-1}). It is implied that in this molar flux range, the reaction time was long enough to allow efficient collisions between $^1O_2$ and E2, resulting in 'full' E2 elimination (note that the removal is not complete because a 100 % yield of reaction is not typically possible in experiments). A linear increase in rate of disappearance was observed for the low E2 molar flux range (0.47 – 9.3 nmol L^{-1} s^{-1}) as the rate of disappearance was inversely proportional to the hydraulic residence time.

However, E2 removal decreased when the molar flux increased from 9.3 to 23 nmol L^{-1} s^{-1} corresponding to a water flux increase from 1200 to 3000 L m^{-2} h^{-1}. In this flux range, the hydraulic residence time (below 0.05 s) limited the collisions. The rate of disappearance levelled off at around 7 ± 2 nmol L^{-1} s^{-1}, which is roughly equal to the molar flux of E2, above which the removal started decreasing (9.3 nmol L^{-1} s^{-1}). Essentially, within a specific reaction time, the number of collisions does not surpass the number of reactant (E2) molecules, and hence, a maximum collision frequency that led to reaction (*i.e.* maximum effective collision frequency Z_{eff}) is determined at an E2 molar flux of around 9 nmol L^{-1} s^{-1}. If the rate of disappearance (7 ± 2 nmol L^{-1} s^{-1}) is assumed to be equal to Z_{eff}, an efficiency factor was determined to be 11 % since the total collision frequency is 64 ± 5 nmol L^{-1} s^{-1}. While other factors (light intensity, PdTFPP loading, and light absorption) seemed to be not limiting, this efficiency factor may correspond to a steric factor β of one order of magnitude, as the $^1O_2$ preferentially attacks electron-rich moieties [52,53], such as the aromatic rings, and does not tend to react with other moieties of the E2 chemical structure. A similar steric factor had been reported for reactions between small molecules only at well-defined reaction centres [40].

The effective collision frequency is specific for E2 as reactions between $^1O_2$ and other micropollutant molecules (with varied chemical structures) may yield different values. The selectivity towards steroid hormone molecules that contain aromatic moieties was be investigated in the next section.

3.5. Explanation of selectivity with collision effectiveness

Reactions between $^1O_2$ and non-aromatic micropollutants (with lower reaction rates) are not considered purely diffusion-controlled; the observed rate is related to both the Smoluchowski diffusion rate (k_{Smol}) and the activation-dependent rate of reaction between encountered reactants in a reactive boundary [95]. The selectivity towards aromatic reactants was examined in experiments with varied steroid hormone types (E1, E2, T and P). These molecules have slightly varied molecular weights (270 – 314 g mol^{-1}); hence, similar total collision frequencies between the steroid hormones and $^1O_2$ were obtained (60 – 70 nmol L^{-1} s^{-1}). Because the PCMs adsorbed E1 and P better than T and E2, the membranes needed to be pre-saturated with E1 and P by filtration with 700 mL in the dark phase prior to the main experiment (with both the dark and light phases). Steroid hormone removal in the main experiments is shown in Fig. 8. The experimental parameters are shown in Fig. S28.

From Fig. 8 A, with pre-saturation of E1 and P, the adsorption saturation for all four hormones was achieved within the dark phase, and a steady state concentration was reached within 600 mL in the light phase. Fig. 8 B shows that the removal of T and P was insignificant: because the error is higher than the average removal value, it is implied that the true removal can be as low as 0 %. In contrast, the removal of E1 and E2 (which contain phenolic rings for $^1O_2$ attack) was significant, at

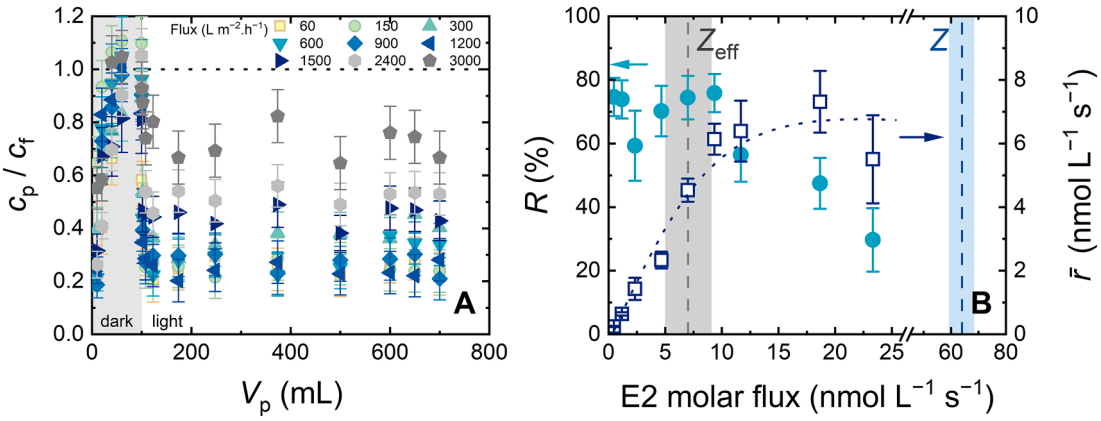

Fig. 7. c_p/c_f as a function of V_p (A); R and $\bar{r}$ as functions of E2 molar flux (B). PdTFPP loading 50 ± 10 μmol g^{-1}, light intensity 14 mW cm^{-2}, 100 ± 10 ng/L E2, 10 mmol L^{-1} NaCl, 1 mmol L^{-1} $NaHCO_3$, 8.5 ± 0.3 mg L^{-1} dissolved oxygen, pH 8.2 ± 0.1. The dark and light grey boxes indicate the frequencies of total collisions Z (64 ± 5 nmol L^{-1} s^{-1}) and successful collisions Z_{eff} (7 ± 2 nmol L^{-1} s^{-1}), respectively.

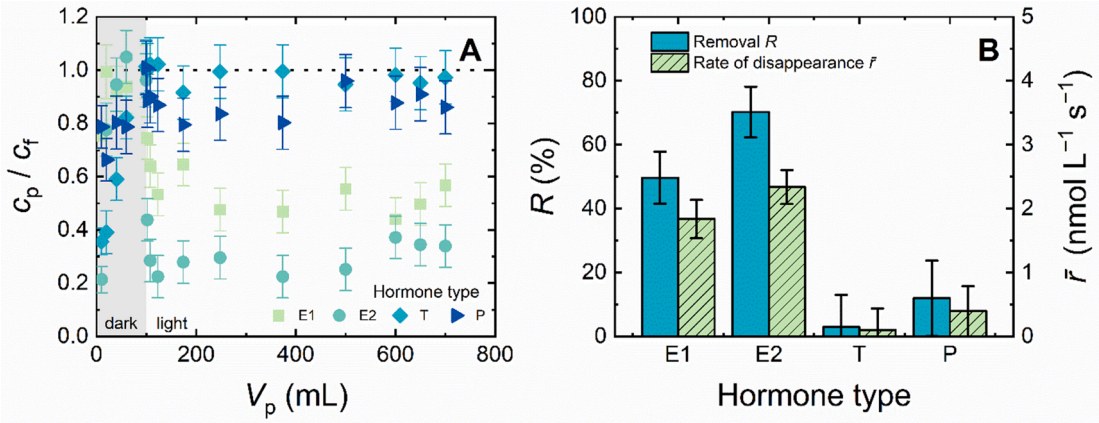

Fig. 8. c_p/c_f as a function of V_p (A); R and $\bar{r}$ *vs.* hormone type (B). PdTFPP loading 50 ± 10 μmol g^{-1}, light intensity 14 mW cm^{-2}, flux 600 L m^{-2} h^{-1}, 100 ± 10 ng L^{-1} hormone, 10 mmol L^{-1} NaCl, 1 mmol L^{-1} $NaHCO_3$, 8.5 ± 0.3 mg L^{-1} dissolved oxygen, pH 8.2 ± 0.1.

(50 ± 8) % and (72 ± 8) %, respectively, implying that more collisions led to reaction in the cases of E1 and E2 than the cases of T and P. A low activation energy allows very fast reaction between encountered reactants (such as $^1O_2$ and E1/E2), and the overall reaction rate is limited only by diffusion following the Smoluchowski collision theory. If the rate of disappearance is equal to the effective collision frequency, the percentage of collisions that led to reaction was 4 – 6 % for E2, and ~ 0 % for T and P. It is noted that these values are not equal to the 'steric factors' related to the probability of $^1O_2$ to find the target bonds, because the steric factor was only calculated when the steroid hormone molar flux was no longer limiting. However, the zero removal of T and P may imply that a significant activation energy would be required to break the olefin π-bond (C = C), although this reaction is feasible [96].

It is noted that the state of reaction between $^1O_2$ and T/P may vary with PCM process conditions. Lyubimenko *et al.* achieved a partial (55 %) removal of T with a PdTFPP-coated PVDF PCM although the pore diameter was smaller (20 nm), by applying higher light intensity (81.0 mW cm^{-2}) and lower flux (60 L m^{-2} h^{-1}) [61]. The stronger confinement in these 20 nm diameter pores may allow closer contact between $^1O_2$ and T as well as more collisions between T with the pore wall and $^1O_2$ on the PdTFPP surface. These phenomena, together with the lower molar flux of T (in the order of 0.5 nmol L^{-1} s^{-1} compared to 4.7 nmol L^{-1} s^{-1} in this work) allow repeated collisions between $^1O_2$ and T for some successful reactions. A strong nanoconfinement that restricts molecular orientation should not be experienced at this scale of pore diameter (for that, pore diameters of several nanometres are required) [29]. The removal of P reported by Lyubimenko *et al.* with the same membrane and experimental conditions was insignificant [61].

3.6. Collision frequency in optimised experiment

In an attempt to attain a higher steroid hormone (E2) removal, an optimised photocatalytic experiment was performed with a lower water flux (60 L m^{-2} h^{-1}, corresponding to an E2 molar flux in the order of 0.5 nmol L^{-1} s^{-1}), higher PdTFPP loading (88 ± 8 μmol g^{-1}) and stronger light intensity (81.5 mW cm^{-2}) to ensure that a vast excess of $^1O_2$ was present while the reaction time was sufficiently long. The relative E2 concentration, removal, and rate of disappearance *vs.* permeate volume in this experiment are shown in Fig. 9.

From Fig. 9 A, in the optimised experiment, the adsorption saturation was achieved within 100 mL of the dark phase, and a steady state concentration was reached within 600 mL in the light phase. The steady state removal attained for the optimised was around 85 % (Fig. 9 B), which is higher than the removal (72%) attained for the 'normal' experiment with a PdTFPP loading of 50 ± 10 μmol g^{-1}, light intensity of 14 mW cm^{-2}, and water flux of 600 L m^{-2} h^{-1}. As observed in Fig. 9 C,

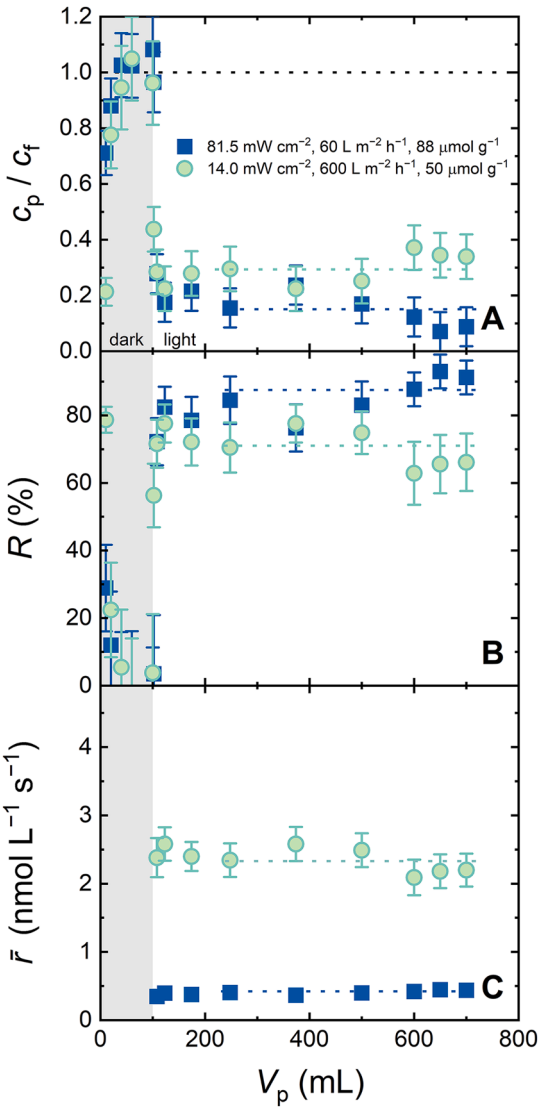

Fig. 9. c_p/c_f (A), R (B) and $\bar{r}$ (C) as functions of V_p in a 'normal' experiment (PdTFPP loading 50 ± 10 μmol g^{-1}, light intensity 14 mW cm^{-2}, water flux 600 L m^{-2} h^{-1}) and an optimised experiment (PdTFPP loading 88 ± 8 μmol g^{-1}, light intensity 81.5 mW cm^{-2}, water flux 60 L m^{-2} h^{-1}). Common conditions: 100 ± 10 ng L^{-1} E2, 10 mM NaCl, 1 mM $NaHCO_3$, 8.5 ± 0.3 mg L^{-1} dissolved oxygen, pH 8.2 ± 0.1.

the rate of disappearance in the optimised experiment was approximately 10 times lower than that of the 'normal' experiment because of the longer hydraulic residence time. It appears that the optimisation resulted only in a moderate improvement in removal. Because the incident light intensity was no longer a limiting factor to $^1O_2$ generation at above 14 mW cm^{-2}, it is expected that the quantity of $^1O_2$ generated in the optimised experiment reached the threshold of 17 nmol L^{-1}, and the total collision frequency was at 64 nmol L^{-1} s^{-1}, similar to that in the 'normal' experiment. The lower water and E2 molar fluxes in the optimised experiment allow longer reaction time between E2 and $^1O_2$, although the molar fluxes in both optimised and normal experiments (0.5 and 4.7 nmol L^{-1} s^{-1}) were lower than the effective collision frequency threshold (which was determined in the previous sections to be around 7 nmol L^{-1} s^{-1}, 11 % of the total collision frequency). It is implied that the lower water flux did not result in an increased frequency of collisions. However, a 13 % higher E2 removal was observed with the optimised experiment, which suggests that the collisions were more effective under the combination of low convective flow, strong light irradiance, and high PdTFPP loading.

3.7. Application of collision theory in varied diameters of nanopores

Based on the above findings for 200 nm diameter pores of PdTFPP-PTFE membranes, the performance of micropollutant (steroid hormone) photodegradation can be explained by the collision theory for varied pore diameters. The reaction zone that experiences wall effects (*i.e.* solute–wall interaction/adsorption), the reaction zone, and the zone without reaction (to where reactive oxygen species cannot diffuse) are schematically described in Fig. 10 for varied diameters of pores. Micropollutant molecules are transported towards the pore wall by diffusion. However, when the molecules are very near the polymer surface inside the pores (~ 1 nm), solute–wall interactions (*e.g.* van der Waals force and hydrogen bonding) become significant, keeping the molecules attracted (or adsorbed) to the pore surface. Within this narrow zone (orange), reactivity is likely to be enhanced as reactants are more concentrated depending on the affinity between the pore surface and molecules. In the reaction zone (yellow), the reactants ($^1O_2$ and steroid hormone molecules) can react in the liquid phase. The zone without reaction (blue) is where $^1O_2$ cannot be found, as these species self-decay before they can diffuse a significant distance of several micrometres (with a lifetime of 3 μs [80], the average self-diffusion distance of $^1O_2$ is around 270 nm [82], although this distance may not be unidirectional).

Pore diameters in the order of 1 nm and 10 nm (Fig. 10 A and B, not relevant in this work as too small) experience significant wall effects, as the reaction zone (orange colour) is a relatively large proportion of the space inside these pores. The walls affect the photocatalytic reactivity because the pollutants are drawn towards the walls where reactive species are generated, which results in a possible uneven distribution of concentrations of both reactants with distance from the pores (*i.e.* higher reactivity at the pore walls and lower reactivity at the pore centre) [26–28]. These pore diameter scales are not included in the current study, although in a previous work (Lyubimenko *et al.*), higher reaction rates in ~20 nm diameter nanopores compared to ~200 nm diameter nanopores have been observed [61].

In a 200 nm pore (Fig. 10 C), which is the relevant scale to the photocatalytic membranes investigated, the zone under direct wall interactions is relatively small (0.5 % of the space inside a pore). If the affinity of the pore surface towards the micropollutants is relatively weak, the reactants (singlet oxygen and micropollutants) can diffuse in the liquid phase. It is noted that the lifetime of $^1O_2$ is relatively long that allows a long diffusion distance; if other reactive species with shorter lifetimes are involved, reactivity would be limited to the proximity to the pore wall due to shorter diffusion distances, resulting in a stronger variation in collision frequency in the radial direction.

In larger pores (Fig. 10 D and E, not relevant in this work), the concentration of $^1O_2$ reduces exponentially with increasing distance from the pore walls (with a lifetime of 3 μs [80], the average self-diffusion distance of $^1O_2$ is around 270 nm [82]). Only the steroid hormone molecules that diffuse towards the vicinity of the pore walls (*e.g.* < 500 nm) can react with $^1O_2$, while those located at the pore centre exit the pores without reacting. Consequently, the photocatalytic reactivity is lower in larger pores compared to the smaller ones. The collision theory remains relevant, but it must account for the lack of reactive species at the centre of the pores, where collisions would not occur and thus no pollutants can be degraded. The smaller pore diameters would be required for effective photocatalysis.

4. Conclusions

In summary, the PdTFPP-PTFE membranes are suitable PCMs to establish a collision theory framework for elucidating the process

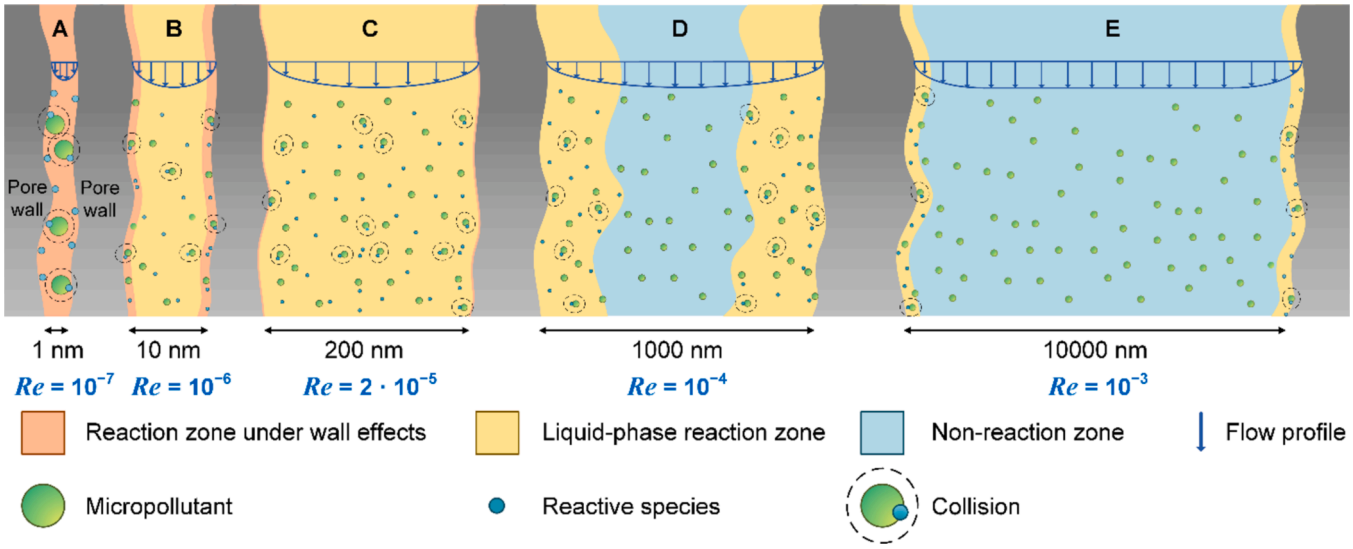

Fig. 10. Flow profiles, reaction zones and zones without reaction inside the pores of different diameters (A: 1 nm, B: 10 nm, C: 200 nm, D: 1000 nm, and E: 10,000 nm). The Reynolds numbers (*Re*) are given. The pore diameters are not to scale. The pore, micropollutant and reactive species diameters are not to scale. The photocatalyst/PS coatings are not shown. The reaction zone under wall effects (~1 nm in radial distance) is narrow and not visible in D and E.

performance limitations. The assessment of this collision theory was made *via* quantifying the $^1O_2$ generated through photon conversion in the PCM. The collision frequency (which is an indicator of reaction rate) between $^1O_2$ and steroid hormone E2 was found to be limited by a light intensity up to 14 mW cm^{-2} and PdTFPP loading up to 31 μmol g^{-1}. By stacking the PCMs, it was discovered that the majority of photons were absorbed by the top-most PCM layer, and hence increasing the membrane layer thickness does not correlate with increased collision frequency and better E2 removal. When the reaction time was restricted by reducing the water and E2 molar fluxes, a maximum effective collision frequency was determined (at around 7 nmol L^{-1} s^{-1}), which corresponds to a steric factor of 11 %. This means 11 % of collisions led to successful reaction. The effectiveness of collisions was then examined for other steroid hormones (E1, T, and P) to highlight the selectivity of $^1O_2$ towards aromatic moieties.

While the collision theory offers novel insights into the fundamental mechanisms and limitations of photodegradation in PdTFPP-PTFE membranes, the translation of this framework to other reactive nanopore systems will necessitate experimental and modelling efforts. For example, the presence of other reactive species, such as hydroxyl radicals (•OH), superoxide anion ($•O_2^-$) and methyl radicals ($•CH_3$) generated from the photo-excitation of TiO_2 photocatalysts, may induce micro-electric effects due to their charges [97], and introduce competition for reaction with micropollutant molecules as well as different quenching pathways. This work solely focused on aqueous-phase reactions in 200 nm diameter pores; smaller (*i.e.* more confining) nanopores may exhibit stronger wall effects (such as micropollutant adsorption/desorption and sorbed-phase reaction). The steric effect (steric factor β is equal to 11 % for E2) can be overcome by reducing the exposed micropollutant surface for ROS attack in spatial nanoconfinement. The tortuous nature of pores was not considered in this work, although this may result in improved light scattering for ROS generation and more collisions between micropollutants and ROS deposited on the pore surface. Nevertheless, all the above challenges can be addressed within the collision theory framework.

PCMs, which combine membrane filtration and photocatalysts/PS for the degradation of recalcitrant micropollutants, show great promise for water purification applications. However, their development has so far been limited to small-scale laboratory setups, with a wide range of reactor designs, configurations, flow dynamics, and integrations having been reported. The collision theory framework introduced in this study offers novel insights for predicting photodegradation performance and identifying process limitations related to mass transfer and light delivery in diverse types of PCMs. Therefore, this framework could contribute to the advancement of materials and chemical engineering.

CRediT authorship contribution statement

Minh N. Nguyen: Writing – original draft, Validation, Methodology, Investigation, Formal analysis, Data curation, Conceptualization. **Camila S. Raota:** Writing – review & editing, Investigation, Formal analysis. **Andrey Turshatov:** Writing – review & editing, Supervision, Methodology, Formal analysis. **Bryce S. Richards:** Writing – review & editing, Supervision, Methodology, Formal analysis. **Andrea I. Schäfer:** Writing – review & editing, Validation, Supervision, Conceptualization.

Declaration of competing interest

The authors declare that they have no known competing financial interests or personal relationships that could have appeared to influence the work reported in this paper.

Acknowledgements

The Helmholtz Association is acknowledged for supporting the research infrastructure through i) the Recruitment Initiative (both A.I.S. and B.S.R.) and ii) the Research Field Energy > Program “Materials and Technologies for the Energy Transition” – Topic 1: Photovoltaics 38.01.05 (B.S.R.). The German Research Foundation (DFG) is acknowledged for project funding (SOLEMBA, project number 500108120). *Coordenação de Aperfeiçoamento Pessoal de Nível Superior* (CAPES), Brazil, and the German Academic Exchange Service (DAAD), Germany, are acknowledged for providing the PDSE and STIBET Contact scholarships, respectively, for the research stay of C.S.R. Open Access funding was enabled and organised by Projekt DEAL. Merck Millipore Corp. is appreciated for supplying the support membranes (PTFE). Aleksandra Orlova and Eduard Madirov (IMT, KIT) are thanked for assistance with the preparation of porphyrin-coated membranes and optical measurements of the membranes, respectively. Margarete Offermann (IAM-ESS, KIT, who has now retired) is appreciated for the membrane porosity measurements with helium pycnometry. Roman Lyubimenko and Siqi Liu (IAMT, KIT) are appreciated for critical discussions related to photocatalytic membrane reactors. Yang-Hui Cai and Jennifer Quiros-Jimenez (IAMT, KIT) are thanked for discussions about membrane characterisation.

Appendix A. Supplementary data

Supplementary data to this article can be found online at https://doi.org/10.1016/j.cej.2024.157582.

Data availability

Data will be made available on request.

References

[1] M. Salgot, M. Folch, Wastewater treatment and water reuse, Curr. Opin. Environ. Sci. Health 2 (2018) 64–74, https://doi.org/10.1016/j.coesh.2018.03.005.
[2] WHO/UNICEF, Progress on drinking water, sanitation and hygiene (WASH), https://washdata.org/, accessed on 12 November 2024.
[3] T.A. Larsen, S. Hoffmann, C. Lüthi, B. Truffer, M. Maurer, Emerging solutions to the water challenges of an urbanizing world, Science 352 (2016) 928–933, https://doi.org/10.1126/science.aad8641.
[4] J. Margot, L. Rossi, D.A. Barry, C. Holliger, A review of the fate of micropollutants in wastewater treatment plants, WIREs: Water 2 (2015) 457–487, https://doi.org/10.1002/wat2.1090.
[5] N.H. Tran, M. Reinhard, K.-Y.-H. Gin, Occurrence and fate of emerging contaminants in municipal wastewater treatment plants from different geographical regions - A review, Water Res. 133 (2018) 182–207, https://doi.org/10.1016/j.watres.2017.12.029.
[6] R.I.L. Eggen, J. Hollender, A. Joss, M. Schärer, C. Stamm, Reducing the discharge of micropollutants in the aquatic environment: The benefits of upgrading wastewater treatment plants, Environ. Sci. Technol. 48 (2014) 7683–7689, https://doi.org/10.1021/es500907n.
[7] World Health Organization, Potable reuse: Guidance for producing safe drinking-water, https://www.who.int/publications/i/item/9789241512770, accessed on 12 November 2024.
[8] B. Haist-Gulde, G. Baldauf, H.J. Brauch, Removal of organic micropollutants by activated carbon, in: J. Hrubec, Water Pollution: Drinking Water and Drinking Water Treatment, Springer, Berlin, Heidelberg, 1995, pp. 103–128.
[9] K. Arola, B. Van der Bruggen, M. Mänttäri, M. Kallioinen, Treatment options for nanofiltration and reverse osmosis concentrates from municipal wastewater treatment: a review, Crit. Rev. Environ. Sci. Technol. 49 (2019) 2049–2116, https://doi.org/10.1080/10643389.2019.1594519.
[10] D.B. Miklos, C. Remy, M. Jekel, K.G. Linden, J.E. Drewes, U. Hübner, Evaluation of advanced oxidation processes for water and wastewater treatment – A critical review, Water Res. 139 (2018) 118–131, https://doi.org/10.1016/j.watres.2018.03.042.
[11] W. Sun, H. Dong, Y. Wang, S. Duan, W. Ji, H. Huang, J. Gu, Z. Qiang, Ultraviolet (UV)-based advanced oxidation processes for micropollutant abatement in water treatment: gains and problems, J. Environ. Chem. Eng. 11 (2023) 110425, https://doi.org/10.1016/j.jece.2023.110425.
[12] C. Dong, W. Fang, Q. Yi, J. Zhang, A comprehensive review on reactive oxygen species (ROS) in advanced oxidation processes (AOPs), Chemosphere 308 (2022) 136205, https://doi.org/10.1016/j.chemosphere.2022.136205.
[13] R. Molinari, M. Mungari, E. Drioli, A. Di Paola, V. Loddo, L. Palmisano, M. Schiavello, Study on a photocatalytic membrane reactor for water purification, Catal. Today 55 (2000) 71–78, https://doi.org/10.1016/S0920-5861(99)00227-8.
[14] S. Mozia, Photocatalytic membrane reactors (PMRs) in water and wastewater treatment. A review, Sep. Purif. Technol. 73 (2010) 71–91, https://doi.org/10.1016/j.seppur.2010.03.021.

[15] R. Molinari, C. Lavorato, P. Argurio, The evolution of photocatalytic membrane reactors over the last 20 years: A state of the art perspective, Catalysts 11 (2021) 775, https://doi.org/10.3390/catal11070775.

[16] C. Michelin, N. Hoffmann, Photosensitization and photocatalysis—perspectives in organic synthesis, ACS Catal. 8 (2018) 12046–12055, https://doi.org/10.1021/acscatal.8b03050.

[17] R.R. Allison, C.H. Sibata, Oncologic photodynamic therapy photosensitizers: a clinical review, Photodiagn. Photodyn. Ther. 7 (2010) 61–75, https://doi.org/10.1016/j.pdpdt.2010.02.001.

[18] R. Lyubimenko, O.I. Gutierrez Cardenas, A. Turshatov, B.S. Richards, A.I. Schäfer, Photodegradation of steroid-hormone micropollutants in a flow-through membrane reactor coated with Pd(II)-porphyrin, Appl. Catal. B: Environ. 291 (2021) 120097, https://doi.org/10.1016/j.apcatb.2021.120097.

[19] S. Silvestri, A.R. Fajardo, B.A. Iglesias, Supported porphyrins for the photocatalytic degradation of organic contaminants in water: a review, Environ. Chem. Lett. 20 (2022) 731–771, https://doi.org/10.1007/s10311-021-01344-2.

[20] Y. Li, X. Wang, Z. Li, M. Chen, J. Zheng, X. Wang, Recent advances in photocatalytic membranes for pharmaceuticals and personal care products removal from water and wastewater, Chem. Eng. J. 475 (2023) 146036, https://doi.org/10.1016/j.cej.2023.146036.

[21] Kirby B., Stokes flow, in: Micro- and nanoscale fluid mechanics : Transport in microfluidic devices, Cambridge University Press, New York, 178-198 (2010).

[22] J.A. LaVerne, The production of OH radicals in the radiolysis of water with ^{4}He ions, Radiat. Res. 118 (1989) 201–210, https://doi.org/10.2307/3577437.

[23] G.V. Buxton, C.L. Greenstock, W.P. Helman, A.B. Ross, Critical review of rate constants for reactions of hydrated electrons, hydrogen atoms and hydroxyl radicals (·OH/·O$^-$) in aqueous solution, J. Phys. Chem. Ref. Data 17 (1988) 513–886, https://doi.org/10.1063/1.555805.

[24] J. Zhang, Y. Nosaka, Mechanism of the OH radical generation in photocatalysis with TiO_2 of different crystalline types, J. Phys. Chem. C 118 (2014) 10824–10832, https://doi.org/10.1021/jp501214m.

[25] S. Zhang, X. Quan, D. Wang, Fluorescence microscopy image-analysis (FMI) for the characterization of interphase HO˙ production originated by heterogeneous catalysis, Chem. Commun. 53 (2017) 2575–2577, https://doi.org/10.1039/C6CC09536D.

[26] S. Zhang, M. Sun, T. Hedtke, A. Deshmukh, X. Zhou, S. Weon, M. Elimelech, J.-H. Kim, Mechanism of heterogeneous Fenton reaction kinetics enhancement under nanoscale spatial confinement, Environ. Sci. Technol. 54 (2020) 10868–10875, https://doi.org/10.1021/acs.est.0c02192.

[27] S. Zhang, T. Hedtke, L. Wang, X. Wang, T. Cao, M. Elimelech, J.-H. Kim, Engineered nanoconfinement accelerating spontaneous manganese-catalyzed degradation of organic contaminants, Environ. Sci. Technol. 55 (2021) 16708–16715, https://doi.org/10.1021/acs.est.1c06551.

[28] W. Zhang, S. Zhang, C. Meng, Z. Zhang, Nanoconfined catalytic membranes assembled by cobalt-functionalized graphitic carbon nitride nanosheets for rapid degradation of pollutants, Appl. Catal. B: Environ. 322 (2023) 122098, https://doi.org/10.1016/j.apcatb.2022.122098.

[29] B. Dong, Y. Pei, N. Mansour, X. Lu, K. Yang, W. Huang, N. Fang, Deciphering nanoconfinement effects on molecular orientation and reaction intermediate by single molecule imaging, Nat. Commun. 10 (2019) 1–6, https://doi.org/10.1038/s41467-019-12799-x.

[30] A.B. Grommet, M. Feller, R. Klajn, Chemical reactivity under nanoconfinement, Nat. Nanotechnol. 15 (2020) 256–271, https://doi.org/10.1038/s41565-020-0652-2.

[31] J.P. Thiruraman, D.P. Masih, M. Drndić, Ions and water dancing through atom-scale holes: a perspective toward “size zero”, ACS Nano 14 (2020) 3736–3746, https://doi.org/10.1021/acsnano.0c01625.

[32] J. Yguerabide, M.A. Dillon, M. Burton, Kinetics of diffusion-controlled processes in liquids. Theoretical consideration of luminescent systems: Quenching and excitation transfer in collision, J. Chem. Phys. 40 (1964) 3040–3052, https://doi.org/10.1063/1.1724945.

[33] A.J. Orr-Ewing, Dynamics of bimolecular reactions in solution, Annu. Rev. Phys. Chem. 66 (2015) 119–141, https://doi.org/10.1146/annurev-physchem-040214-121654.

[34] S. Arrhenius, Über die Dissociationswärme und den Einfluss der Temperatur auf den Dissociationsgrad der Elektrolyte, Z. Phys. Chem. 4U (1889) 96–116, https://doi.org/10.1515/zpch-1889-0408.

[35] F.B. Knight, On the random walk and Brownian motion, Trans. Am. Math. Soc. 103 (1962) 218–228, https://doi.org/10.1090/S0002-9947-1962-0139211-2.

[36] D.F. Calef, J.M. Deutch, Diffusion-controlled reactions, Annu. Rev. Phys. Chem. 34 (1983) 493–524, https://doi.org/10.1146/annurev.pc.34.100183.002425.

[37] M. v. Smoluchowski, Versuch einer mathematischen Theorie der Koagulationskinetik kolloider Lösungen, Z. Phys. Chem. 92 (1917) 129–168, https://doi.org/10.1515/zpch-1918-9209.

[38] S.H. Northrup, H.P. Erickson, Kinetics of protein−protein association explained by Brownian dynamics computer simulation, Proc. Natl. Acad. Sci. U.S.A. 89 (1992) 3338–3342, https://doi.org/10.1073/pnas.89.8.3338.

[39] M. Schlosshauer, D. Baker, Realistic protein-protein association rates from a simple diffusional model neglecting long-range interactions, free energy barriers, and landscape ruggedness, Protein Sci. 13 (2004) 1660–1669, https://doi.org/10.1110/ps.03517304.

[40] T. Arita, O. Kajimoto, M. Terazima, Y. Kimura, Experimental verification of the Smoluchowski theory for a bimolecular diffusion-controlled reaction in liquid phase, J. Chem. Phys. 120 (2004) 7071–7074, https://doi.org/10.1063/1.1683071.

[41] S.D. Traytak, Diffusion-controlled reaction rate to an active site, Chem. Phys. 192 (1995) 1–7, https://doi.org/10.1016/0301-0104(94)00353-C.

[42] K. Šolc, W.H. Stockmayer, Kinetics of diffusion-controlled reaction between chemically asymmetric molecules. II. Approximate steady-state solution, Int. J. Chem. Kinet. 5 (1973) 733–752, https://doi.org/10.1002/kin.550050503.

[43] V.M. Berdnikov, A.B. Doktorov, Steric factor in diffusion-controlled chemical reactions, Chem. Phys. 69 (1982) 205–212, https://doi.org/10.1016/0301-0104(82)88147-0.

[44] T. Hirakawa, Y. Nosaka, Properties of $O_2^{\bullet-}$ and OH$^{\bullet}$ formed in TiO_2 aqueous suspensions by photocatalytic reaction and the influence of H_2O_2 and some ions, Langmuir 18 (2002) 3247–3254, https://doi.org/10.1021/la015685a.

[45] M.S. Baptista, J. Cadet, P. Di Mascio, A.A. Ghogare, A. Greer, M.R. Hamblin, C. Lorente, S.C. Nunez, M.S. Ribeiro, A.H. Thomas, M. Vignoni, T.M. Yoshimura, Type I and type II photosensitized oxidation reactions: Guidelines and mechanistic pathways, Photochem. Photobiol. 93 (2017) 912–919, https://doi.org/10.1111/php.12716.

[46] S. Yu, R.-X. Zhu, K.-K. Niu, N. Han, H. Liu, L.-B. Xing, Switchover from singlet oxygen to superoxide radical through a photoinduced two-step sequential energy transfer process, Chem. Sci. 15 (2024) 1870–1878, https://doi.org/10.1039/D3SC05820D.

[47] H. Wang, Z. Yang, K. Zhang, W. Wang, F. Lin, H. Huang, W. Qin, Z. Chi, Z. Yang, New Janus organic Type-I photosensitizer capable of transforming glutathione from opponent to ally for assisting photodynamic therapy, ACS Mater. Lett. 6 (2024) 1317–1326, https://doi.org/10.1021/acsmaterialslett.3c01210.

[48] F. Xu, X.-N. Song, G.-P. Sheng, H.-W. Luo, W.-W. Li, R.-S. Yao, H.-Q. Yu, Vitamin B2-initiated hydroxyl radical generation under visible light in the presence of dissolved iron, ACS Sustain. Chem. Eng. 3 (2015) 1756–1763, https://doi.org/10.1021/acssuschemeng.5b00267.

[49] Dumoulin F., Design and conception of photosensitisers, in: T. Nyokong, V. Ahsen, Photosensitizers in Medicine, Environment, and Security, Springer Netherlands, Dordrecht, 1-46 (2012).

[50] E.F.F. Silva, C. Serpa, J.M. Dąbrowski, C.J.P. Monteiro, S.J. Formosinho, G. Stochel, K. Urbanska, S. Simões, M.M. Pereira, L.G. Arnaut, Mechanisms of singlet-oxygen and superoxide-ion generation by porphyrins and bacteriochlorins and their implications in photodynamic therapy, Chemistry – A European Journal 16 (2010) 9273–9286, https://doi.org/10.1002/chem.201000111.

[51] R. Lyubimenko, B.S. Richards, A.I. Schäfer, A. Turshatov, Noble-metal-free photosensitizers for continuous-flow photochemical oxidation of steroid hormone micropollutants under sunlight, J. Membr. Sci. 642 (2022) 119981, https://doi.org/10.1016/j.memsci.2021.119981.

[52] M.C. DeRosa, R.J. Crutchley, Photosensitized singlet oxygen and its applications, Coord. Chem. Rev. 233–234 (2002) 351–371, https://doi.org/10.1016/S0010-8545(02)00034-6.

[53] Y. Lee, U. von Gunten, Oxidative transformation of micropollutants during municipal wastewater treatment: Comparison of kinetic aspects of selective (chlorine, chlorine dioxide, ferrate^{VI}, and ozone) and non-selective oxidants (hydroxyl radical), Water Res. 44 (2010) 555–566, https://doi.org/10.1016/j.watres.2009.11.045.

[54] F. Wilkinson, W.P. Helman, A.B. Ross, Rate constants for the decay and reactions of the lowest electronically excited singlet state of molecular oxygen in solution. An expanded and revised compilation, J. Phys. Chem. Ref. Data 24 (1995) 663–677, https://doi.org/10.1063/1.555965.

[55] H. Ali, J.E. van Lier, Metal complexes as photo- and radiosensitizers, Chem. Rev. 99 (1999) 2379–2450, https://doi.org/10.1021/cr980439y.

[56] D.M. Guldi, T.D. Mody, N.N. Gerasimchuk, D. Magda, J.L. Sessler, Influence of large metal cations on the photophysical properties of texaphyrin, a rigid aromatic chromophore, J. Am. Chem. Soc. 122 (2000) 8289–8298, https://doi.org/10.1021/ja001578b.

[57] C.M. Marian, Spin–orbit coupling and intersystem crossing in molecules, Wires Comput. Mol. Sci. 2 (2012) 187–203, https://doi.org/10.1002/wcms.83.

[58] M. Wang, Y. Zhang, G. Yu, J. Zhao, X. Chen, F. Yan, J. Li, Z. Yin, B. He, Monolayer porphyrin assembled SPSf/PES membrane reactor for degradation of dyes under visible light irradiation coupling with continuous filtration, J. Taiwan Inst. Chem. Eng. 109 (2020) 62–70, https://doi.org/10.1016/j.jtice.2020.02.013.

[59] R. Lyubimenko, D. Busko, B.S. Richards, A.I. Schäfer, A. Turshatov, Efficient photocatalytic removal of methylene blue using a metalloporphyrin–poly (vinylidene fluoride) hybrid membrane in a flow-through reactor, ACS Appl. Mater. Interfaces 11 (2019) 31763–31776, https://doi.org/10.1021/acsami.9b04601.

[60] H. Fang, M. Wang, H. Yi, Y. Zhang, X. Li, F. Yan, L. Zhang, Electrostatic assembly of porphyrin-functionalized porous membrane toward biomimetic photocatalytic degradation dyes, ACS Omega 5 (2020) 8707–8720, https://doi.org/10.1021/acsomega.0c00135.

[61] R. Lyubimenko, A. Turshatov, A. Welle, P.G. Weidler, B.S. Richards, A.I. Schäfer, Enhanced photocatalytic efficiency via improved contact in a solar-driven membrane reactor for steroid hormone removal, Chem. Eng. J. 138449 (2022), https://doi.org/10.1016/j.cej.2022.138449.

[62] M. Gmurek, M. Bizukojć, J. Mosinger, S. Ledakowicz, Application of photoactive electrospun nanofiber materials with immobilized meso-tetraphenylporphyrin for parabens photodegradation, Catal. Today 240 (2015) 160–167, https://doi.org/10.1016/j.cattod.2014.06.015.

[63] D.M. Mafukidze, T. Nyokong, Photocatalytic and solar radiation harvesting potential of a free-base porphyrin-zinc (II) phthalocyanine heterodyad functionalized polystyrene polymer membrane for the degradation of 4-chlorophenol, J. Photochem. Photobiol. A: Chem. 409 (2021) 113142, https://doi.org/10.1016/j.jphotochem.2021.113142.

[64] C.S. Raota, S. Lotfi, R. Lyubimenko, B.S. Richards, A.I. Schäfer, Accelerated ageing method for the determination of photostability of polymer-based photocatalytic membranes, J. Membr. Sci. 686 (2023) 121944, https://doi.org/10.1016/j.memsci.2023.121944.
[65] S. Robinson, P.R. Bérubé, Membrane ageing in full-scale water treatment plants, Water Res. 169 (2020) 115212, https://doi.org/10.1016/j.watres.2019.115212.
[66] L.T. Nyamutswa, B. Zhu, S.F. Collins, D. Navaratna, M.C. Duke, Light conducting photocatalytic membrane for chemical-free fouling control in water treatment, J. Membr. Sci. 604 (2020) 118018, https://doi.org/10.1016/j.memsci.2020.118018.
[67] Y. Shi, J. Huang, G. Zeng, W. Cheng, J. Hu, Photocatalytic membrane in water purification: Is it stepping closer to be driven by visible light? J. Membr. Sci. 584 (2019) 364–392, https://doi.org/10.1016/j.memsci.2019.04.078.
[68] S.S. Chin, K. Chiang, A.G. Fane, The stability of polymeric membranes in a TiO_2 photocatalysis process, J. Membr. Sci. 275 (2006) 202–211, https://doi.org/10.1016/j.memsci.2005.09.033.
[69] E. Giannetti, Thermal stability and bond dissociation energy of fluorinated polymers: A critical evaluation, J. Fluor. Chem. 126 (2005) 623–630, https://doi.org/10.1016/j.jfluchem.2005.01.008.
[70] E.E. Meyer, K.J. Rosenberg, J. Israelachvili, Recent progress in understanding hydrophobic interactions, Proc. Natl. Acad. Sci. U.S.A. 103 (2006) 15739, https://doi.org/10.1073/pnas.0606422103.
[71] R. Lanfranco, F. Giavazzi, M. Salina, G. Tagliabue, E. Di Nicolò, T. Bellini, M. Buscaglia, Selective adsorption on fluorinated plastic enables the optical detection of molecular pollutants in water, Phys. Rev. Appli. 5 (2016) 054012, https://doi.org/10.1103/PhysRevApplied.5.054012.
[72] K. Yin, J. Wu, Q. Deng, Z. Wu, T. Wu, Z. Luo, J. Jiang, J.-A. Duan, Tailoring micro/nanostructured porous polytetrafluoroethylene surfaces for dual-reversible transition of wettability and transmittance, Chem. Eng. J. 434 (2022) 134756, https://doi.org/10.1016/j.cej.2022.134756.
[73] M. Gauch, M. Ließmann, H. Ehlers, D. Ristau, Optical properties of fluorocarbon thin films prepared by ion beam sputtering of PTFE, Optical Interference, Coatings (2013) ThA.2, https://doi.org/10.1364/OIC.2013.ThA.2.
[74] Atkins P.W., de Paula J., Data section, in: Atkins' Physical Chemistry, 8th ed., Oxford University Press, New York, 988-1027 (2006).
[75] A. Habib, S. Wagle, A. Decharat, F. Melandsø, Evaluation of adhesive-free focused high-frequency PVDF copolymer transducers fabricated on spherical cavities, Smart Mater. Struct. 29 (2020) 045026, https://doi.org/10.1088/1361-665x/ab7a3d.
[76] M. Morisue, M. Kawanishi, Y. Miyake, K. Kanaori, K. Tachibana, M. Ohke, M. Kohri, J. Matsui, T. Hoshino, S. Sasaki, Metallic lustrous porphyrin foil with an exceptional refractive index, Macromolecules 56 (2023) 7993–8002, https://doi.org/10.1021/acs.macromol.3c00433.
[77] S. Grenoble, M. Gouterman, G. Khalil, J. Callis, L. Dalton, Pressure-sensitive paint (PSP): Concentration quenching of platinum and magnesium porphyrin dyes in polymeric films, J. Lumin. 113 (2005) 33–44, https://doi.org/10.1016/j.jlumin.2004.08.049.
[78] M. Adams, M. Kozlowska, N. Baroni, M. Oldenburg, R. Ma, D. Busko, A. Turshatov, G. Emandi, M.O. Senge, R. Haldar, C. Wöll, G.U. Nienhaus, B.S. Richards, I. A. Howard, Highly efficient one-dimensional triplet exciton transport in a palladium–porphyrin-based surface-anchored metal–organic framework, ACS Appl. Mater. Interfaces 11 (2019) 15688–15697, https://doi.org/10.1021/acsami.9b03079.
[79] B.S. Richards, D. Hudry, D. Busko, A. Turshatov, I.A. Howard, Photon upconversion for photovoltaics and photocatalysis: A critical review, Chem. Rev. 121 (2021) 9165–9195, https://doi.org/10.1021/acs.chemrev.1c00034.
[80] S.Y. Egorov, V.F. Kamalov, N.I. Koroteev, A.A. Krasnovsky, B.N. Toleutaev, S. V. Zinukov, Rise and decay kinetics of photosensitized singlet oxygen luminescence in water. Measurements with nanosecond time-correlated single photon counting technique, Chem. Phys. Lett. 163 (1989) 421–424, https://doi.org/10.1016/0009-2614(89)85161-9.
[81] F. Tampieri, M.-P. Ginebra, C. Canal, Quantification of plasma-produced hydroxyl radicals in solution and their dependence on the pH, Anal. Chem. 93 (2021) 3666–3670, https://doi.org/10.1021/acs.analchem.0c04906.
[82] E. Skovsen, J.W. Snyder, J.D.C. Lambert, P.R. Ogilby, Lifetime and diffusion of singlet oxygen in a cell, J. Phys. Chem. B 109 (2005) 8570–8573, https://doi.org/10.1021/jp051163i.
[83] Levenspiel O., Chapter 2. Kinetics of Homogeneous Reactions, in: Chemical Reaction Engineering, Third Edition, John Wiley & Sons, 13-37 (1998).
[84] S. Liu, P.C. Edara, A.I. Schäfer, Influence of organic matter on the photocatalytic degradation of steroid hormones by TiO_2-coated polyethersulfone microfiltration membrane, Water Res. 245 (2023) 120438, https://doi.org/10.1016/j.watres.2023.120438.
[85] European Chemicals Agency ECHA, ECHA publishes PFAS restriction proposal, https://echa.europa.eu/-/echa-publishes-pfas-restriction-proposal, accessed on 9 January 2024.
[86] ASTM, ASTM G173-03(2012) - Standard tables for reference solar spectral irradiances: Direct normal and hemispherical on 37° tilted surface, West Conshohocken, PA, 2012.
[87] J. Huo, J. Yong, F. Chen, Q. Yang, Y. Fang, X. Hou, Trapped air-induced reversible transition between underwater superaerophilicity and superaerophobicity on the femtosecond laser-ablated superhydrophobic PTFE surfaces, 1900262, Adv. Mater. Interfaces 6 (2019), https://doi.org/10.1002/admi.201900262.
[88] J. Yong, S.C. Singh, Z. Zhan, F. Chen, C. Guo, Substrate-independent, fast, and reversible switching between underwater superaerophobicity and aerophilicity on the femtosecond laser-induced superhydrophobic surfaces for selectively repelling or capturing bubbles in water, ACS Appl. Mater. Interfaces 11 (2019) 8667–8675, https://doi.org/10.1021/acsami.8b21465.
[89] L. Palacio, P. Prádanos, J.I. Calvo, A. Hernández, Porosity measurements by a gas penetration method and other techniques applied to membrane characterization, Thin Solid Films 348 (1999) 22–29, https://doi.org/10.1016/S0040-6090(99)00197-2.
[90] R. Lyubimenko, B.S. Richards, A. Turshatov, A.I. Schäfer, Separation and degradation detection of nanogram-per-litre concentrations of radiolabelled steroid hormones using combined liquid chromatography and flow scintillation analysis, Sci. Rep. 10 (2020) 7095, https://doi.org/10.1038/s41598-020-63697-y.
[91] S. Liu, D. Jassby, D. Mandler, A.I. Schäfer, Differentiation of adsorption and degradation in steroid hormone micropollutants removal using electrochemical carbon nanotube membrane, Nat. Commun. 95 (2024) 1524, https://doi.org/10.1038/s41467-024-52730-7.
[92] J.B. Birks, An introduction to liquid scintillation counting, and solutes and solvents for liquid scintillation counting, Koch-Light Laboratories, Colnbrook, 1975.
[93] D.F. Ollis, E. Pelizzetti, N. Serpone, Photocatalyzed destruction of water contaminants, Environ. Sci. Technol. 25 (1991) 1522–1529, https://doi.org/10.1021/es00021a001.
[94] A.V. Emeline, V. Ryabchuk, N. Serpone, Factors affecting the efficiency of a photocatalyzed process in aqueous metal-oxide dispersions: Prospect of distinguishing between two kinetic models, J. Photochem. Photobiol. A: Chem. 133 (2000) 89–97, https://doi.org/10.1016/S1010-6030(00)00225-2.
[95] F.C. Collins, G.E. Kimball, Diffusion-controlled reaction rates, J. Colloid Sci. 4 (1949) 425–437, https://doi.org/10.1016/0095-8522(49)90023-9.
[96] A.A. Frimer, The reaction of singlet oxygen with olefins: the question of mechanism, Chem. Rev. 79 (1979) 359–387, https://doi.org/10.1021/cr60321a001.
[97] A. Shu, C. Qin, M. Li, L. Zhao, Z. Shangguan, Z. Shu, X. Yuan, M. Zhu, Y. Wu, H. Wang, Electric effects reinforce charge carrier behaviour for photocatalysis, Energy Environ. Sci. (2024), https://doi.org/10.1039/D4EE01379D.